

High-energy and very high-energy gamma-ray emission from the magnetar SGR 1900+14 neighbourhood

B. Hnatyk, R. Hnatyk, V. Zhdanov, and V. Voitsekhovskiy

Astronomical Observatory of Taras Shevchenko National University of Kyiv, 3 Observatorna str. Kyiv, 04053, Ukraine
e-mail: bohdan_hnatyk@ukr.net

Received date / Accepted date

ABSTRACT

Context. Magnetar wind nebulae (MWNe), created by new-born millisecond magnetars, and magnetar giant flares are PeVatron candidates and even potential sources of ultra high energy ($E > 10^{18}$ eV) cosmic rays (UHECRs). Nonthermal high-energy (HE, $E > 100$ MeV) and very high-energy (VHE, $E > 100$ GeV) γ -ray emission from magnetars' neighbourhoods should be a promising signature of acceleration processes.

Aims. We investigate a possibility of explaining HE and VHE γ -ray emission from the vicinity of the magnetar SGR 1900+14 by cosmic rays accelerated in a Supernova remnant of a magnetar-related Supernova and/or in a MWNe.

Methods. Simulation of the observed HE (the extended *Fermi*-LAT source 4FGL J1908.6+0915e) and VHE (the extended H.E.S.S. source candidate HOTS J1907+091 and the point-like HAWC TeV source 3HWC J1907+085) γ -ray emission, spatially coincident with the magnetar SGR 1900+14, was carried out in the framework of hadronic (pp collisions with a subsequent pion decay) and leptonic (inverse Compton scattering of low energy background photons by ultrarelativistic electrons) models.

Results. We show that under reasonable assumptions about parameters of the circumstellar medium the observed γ -ray emission of *Fermi*-LAT 4FGL J1908.6+0915e, H.E.S.S. HOTSJ1907+091 and 3HWC J1907+085 sources may be explained or at least considerably contributed by a (still undetected) magnetar-connected Hypernova remnant and/or a MWNe created by new-born millisecond magnetar with a large reserve of rotational energy $E_{rot} \sim 10^{52}$ erg.

Key words. Stars: magnetars – ISM: supernova remnants – gamma rays: general – acceleration of particles – radiation mechanisms: non-thermal – Astrophysics - High Energy Astrophysical Phenomena

1. Introduction

Magnetars are young neutron stars with extremely high magnetic fields $\sim 10^{14} - 10^{15}$ G (Duncan & Thompson 1992; Thompson & Duncan 1995, 1996; Turolla et al. 2015; Mereghetti et al. 2015; Kaspi & Beloborodov 2017; Esposito et al. 2018).

Observed persistent X-ray – γ -ray activity of magnetars manifests in forms of repeated hard X-ray – soft γ -ray flares (soft gamma repeaters, SGRs) (Paczynski 1992; Thompson & Duncan 1995, 1996; Kouveliotou et al. 1998) and persistent/transient quiescent super-luminous X-ray emission, together with short (milliseconds-seconds) bursts and longer (weeks-months) outbursts (anomalous X-ray pulsars, AXPs) (van Paradijs et al. 1995; Thompson & Duncan 1996; Kaspi et al. 2003)

The total magnetar luminosity considerably exceeds ordinary spin-down energy losses and is supported mainly by a decay of magnetar's magnetic energy during a magnetic field evolution inside a neutron star or reconfigurations of magnetospheric fields (Thompson & Duncan 1995, 1996).

Currently the McGill magnetar catalogue (Olausen & Kaspi 2014) contains 29 magnetars: 15 SGRs (11 confirmed, 4 candidates), and 14 AXPs (12 confirmed, 2 candidates). Compared with regular pulsars, magnetars are young and have generally high dipole magnetic fields (in most cases exceeding the quantum critical magnetic field $B_{cr} = m_e^2 c^3 / e \hbar = 4.413 \times 10^{13}$ G), because observed long spin periods P (2 – 12 s) and high spin-down rate \dot{P} ($\sim 10^{-11} - 10^{-10}$ s s $^{-1}$) correspond to surface magnetic fields $B_d \approx 3.2 \times 10^{19} (P \dot{P})^{1/2}$ G = $3.2 \times 10^{14} P_1^{1/2} \dot{P}_{-11}^{1/2}$ G and

characteristic ages $\tau_c = P/(n-1)\dot{P} = 17 P_1 \dot{P}_{-11}^{-1}$ kyr for braking index $n = 3$ (Kouveliotou et al. 1998) (hereafter the physical quantities are expressed by $Q = 10^Q Q_n$ in cgs units, unless specified otherwise).

Initial rotational kinetic energy of a new-born millisecond ($P_i \sim 10^{-3}$ s) magnetar $E_{rot} \approx 2 \times 10^{52} P_{i-3}^{-2}$ erg can manifest in various forms, especially in an additional energization of a Supernova ejecta in Hypernova case owing to an initial magnetic dipole spin-down luminosity $L_{sd,i} \approx 10^{49} B_{15}^2 P_{i-3}^{-4}$ erg s $^{-1}$ with an initial spin-down timescale $t_{sd,i} = E_{rot}/L_{sd,i} \approx 2 \times 10^3 B_{15}^{-2} P_{i-3}^2$ s (Duncan & Thompson 1992; Bucciantini et al. 2007; Sukhbold & Thompson 2017; Angus et al. 2019).

With time, dissipation of a dipolar magnetic field energy ($E_{mag} \approx B^2 R_{NS}^3 / 6 \approx 3 \times 10^{47} B_{15}^2$ erg for the radius of neutron star $R_{NS} = 12$ km) supplies a X-ray – γ -ray activity of magnetars, including spectacular rare giant flares - the short (~ 0.1 s) hard X-ray – soft γ -ray bursts with luminosities $\sim 10^{44} - 10^{47}$ erg s $^{-1}$ and released energies $\sim 10^{44} - 10^{46}$ erg. Until now, only three such giant flares have been detected (from SGR 0526–66 on 1979 March 5, from SGR 1900+14 on 1998 August 27, and from SGR 1806–20 on 2004 December 27) (Olausen & Kaspi 2014). A sudden release of magnetic energy in over-twisted magnetospheres via solar flare-like fast reconnections creates a GRB-like fireball and an ultrarelativistic (Lorentz factor $\Gamma \leq 10$) outflow (Thompson & Duncan 1995; Parfrey et al. 2013), observed as radio afterglows of the SGR 1900+14 (Frail et al. 1999) and the SGR 1806–20 (Granot et al. 2006) giant flares.

Owing to expected presence of relativistic shock waves and reconnection processes in new-born magnetar winds and magnetar giant flares, magnetars are promising accelerators of relativistic particles with maximum energies in an ultra high energy cosmic ray (UHECR) domain ($E > 10^{18}$ eV) (Eichler 2005; Asano et al. 2006; Liu et al. 2010; Kotera & Olinto 2011; Guépin & Kotera 2017; Fang et al. 2019). As argued in Gnatyk (2018), the magnetar SGR 1900+14 is a potential source of $E > 10^{20}$ eV UHECR triplet (Sokolsky 2014) in view of joint data of Telescope Array (TA) (Abbasi et al. 2014) and Auger (Aab et al. 2015) detectors. Reasonable association SGR 1900+14 with the 4 BCE "po star" (Wang et al. 2002) suggests a Hypernova type of a magnetar-related Supernova with favourable conditions for UHECR acceleration (Kotera & Olinto 2011). If this is the case, the magnetar SGR 1900+14 should also manifest himself as a PeVatron with nonthermal emission in different domains - from radio- to TeV-range (Aharonian 2004; Cherenkov Telescope Array Consortium et al. 2019).

In this work we investigate the expected contribution of the SGR 1900+14-related Supernova remnant (SNR) and/or MWN to the HE and VHE γ -ray emission from the magnetar environment (Fig. 1). We analyse all presently available multi-band observational data concerning the magnetar SGR 1900+14 and its environment and substantiate their explanation in the model of Hypernova-like explosion of a SGR 1900+14 progenitor massive star with dominant energy contribution of the new-born fast rotating magnetar in the Hypernova energy reserve and in MWN formation.

2. Magnetar SGR 1900+14 and its environment

First γ -ray activity (three short ~ 10 ms bursts in 50 – 150 keV energy window with radiated energy $\sim 10^{39}$ erg) of SGR 1900+14 was discovered in 1979 in the Konus experiment aboard the Venera 11 and the Venera 12 space missions (Mazets et al. 1979). In Kouveliotou et al. (1999) a high magnetar-type value of a dipolar magnetic field of SGR 1900+14 $B_d \approx 8 \times 10^{14}$ G and a typical of magnetars young characteristic age $\tau_c \approx 700$ yr were estimated as a consequence of a high observed secular period spin-down $\dot{P} \approx 10^{-10}$ s s $^{-1}$, caused by severe magneto-dipolar energy losses. A giant flare from SGR 1900+14 was detected on 1998 August 27 by set of spacecrafts (Ulysses et al.) in form of a short (~ 1 s) hard (~ 240 keV) extremely intense burst with peak flux $F \geq 3.4 \times 10^{-3}$ erg cm $^{-2}$ s $^{-1}$ and fluence $S \geq 7 \times 10^{-3}$ erg cm $^{-2}$, followed by a long (~ 300 s) tail with a soft energy spectrum and with a 5.16 s period modulation (Hurley et al. 1999). A second, significantly weaker giant flare from SGR 1900+14 was detected on 2001 April 18 (Guidorzi et al. 2001; Hurley et al. 2001).

In contrast to the enhanced activity in the hard X-ray – soft γ -ray range, SGR 1900+14 is undetected yet in other bands (except for the transient radio afterglow of its giant flare, the one that helped to estimate the high-accuracy position for SGR 1900+14 RA $_{2000} = 19^h07^m14^s.33$, Dec $_{2000} = +09^\circ19'20''.1$ (Frail et al. 1999), or $l = 43^\circ.021$, $b = 0^\circ.766$ in Galactic coordinates.

2.1. SGR 1900+14 environment in the radio band

The radio map of SGR 1900+14 region does not display any signatures of the magnetar, as well as of a magnetar-connected SNR or a MWN, only 3 – σ limits on an extended emission of 6.1 mJy arcmin $^{-2}$ (332 MHz) and 6.2 mJy arcmin $^{-2}$ (1.4 GHz) were found in Kaplan et al. (2002) (Figs. 3–7). In the proximity to SGR 1900+14 there are only in radio-band detected shell-type

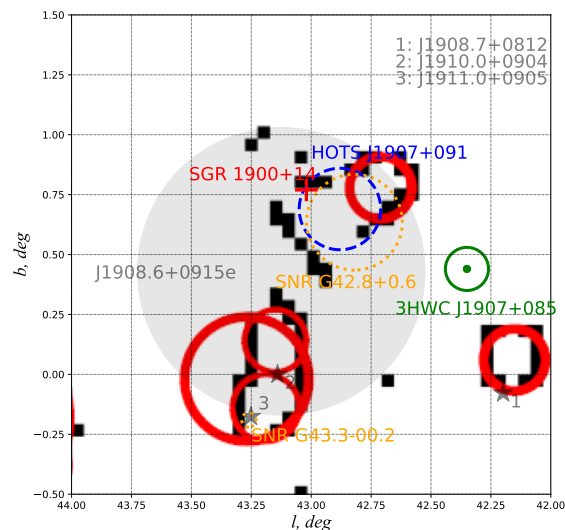


Fig. 1. Magnetar SGR 1900+14 neighbourhood. The red cross indicates the SGR 1900+14 position. The extended 4FGL source J1908.6+0915e (the grey circle) and three point-like 4FGL sources (the grey stars) are also presented together with the H.E.S.S. extended source HOTS J1907+091 (the blue ring) and the HAWC point-like source 3HWC J1907+085 (the green bullet with 1σ error box). Two SNRs in the field are presented by the orange rings. The black filled squares correspond to the edge mask and the red circles to the objects detected in Hough space in H.E.S.S. data, respectively. See text for details.

SNR G42.8+0.6 (of 24' size, $l = 42^\circ.820$, $b = 0^\circ.635$, spectral flux density $F = 2.4 \pm 0.6$ Jy at 1.420 GHz, 2.0 ± 0.2 Jy at 2.695GHz, 1.5 ± 0.2 Jy at 4.750 GHz, spectral index $\alpha = 0.4$) (Fuerst et al. 1987). The angular separation between the magnetar and the centre (boundary) of the SNR G42.8+0.6 is of $\sim 15'$ ($3'$) (Fig. 1). An young ($\tau_c \approx 38$ kyr) $P = 226$ ms radio pulsar PSR J1907+0918 ($l = 43^\circ.024$, $b = 0^\circ.730$ $d = 8.2$ kpc), is a neighbour of SGR 1900+14, the separation between the pulsars $\approx 2'$ (Lorimer & Xilouris 2000; Kaplan et al. 2002).

Despite the young age of both pulsars, none of them are physically connected with the SNR G42.8+0.6, first of allowing to unrealistically high necessary transverse velocity $v_t = 4 \times 10^3 (d_p/10 \text{ kpc}) / (\tau_p/10^4 \text{ yr}) \text{ km s}^{-1}$ for expected distances $d_p \sim 5 - 15$ kpc and ages $\tau_p \sim 10^3 - 4 \times 10^4$ yr of pulsars (Kouveliotou et al. 1999; Lorimer & Xilouris 2000). Once more, the estimated in Tendulkar et al. (2012) proper motion of SGR 1900+14 ($\mu_\alpha, \mu_\delta = (-2.1, -0.6) \pm (0.4, 0.5) \text{ marcsec yr}^{-1}$) corresponds to $v_t = (104 \pm 24) \times (d_p/10 \text{ kpc}) \text{ km s}^{-1}$ and to an approaching to the SNR (Position angle PA = $254^\circ \pm 10^\circ$). Recent estimate of an extinction-based distance to the SNR G42.8+0.6 $d_{ext} = 4.24 \pm 0.93$ pc (Wang et al. 2020) also excludes its physical connection with SGR 1900+14.

2.2. SGR 1900+14 environment in the optical/IR band

Initial searches for a SGR 1900+14 counterpart in an optical/IR domain were unsuccessful: HST/STIS, and Keck J/Ks-band images placed only upper limits of $m_{50CCD} \geq 29^m.0$, $J \geq 22^m.8$, $K_s \geq 20^m.8$ (Kaplan et al. 2002). Only in Testa et al. (2008) a newly detected variable "object # 7" with $K_s \approx 19^m.7$ and $\Delta K_s = 0^m.47 \pm 0^m.11$, observed with ESO-VLT/NACO in the error circle of the SGR 1900+14 radio position, was proposed as a tentative IR candidate counterpart to SGR 1900+14. Later on,

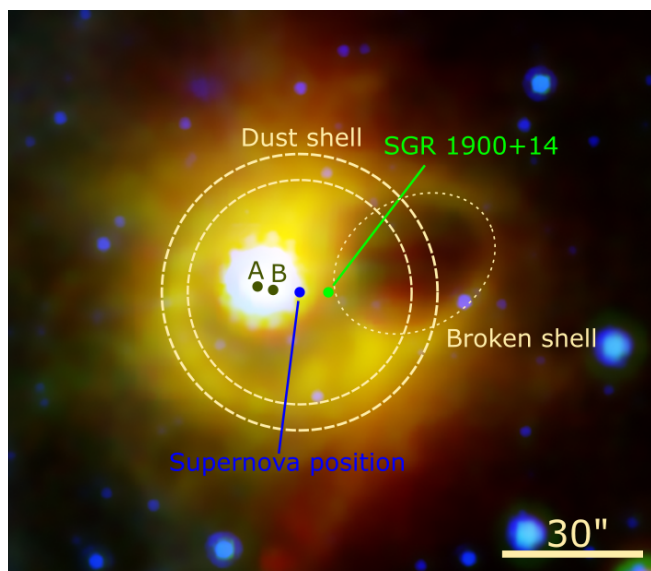


Fig. 2. Spitzer IR map of SGR 1900+14 environment with colour coding: blue ($8 \mu\text{m}$), green ($16 \mu\text{m}$), and red ($24 \mu\text{m}$) (courtesy NASA/JPL/Caltech/S. Wachter (Caltech-SSC)). The green bullet indicates the present magnetar position. The black bullets A and B indicate the positions of two red supergiants at the centre of the open star cluster C11900+14/SGR 1900+14. In our model, the blue bullet in the centre of the observed dust shell (the yellow dashed ring) indicates the Supernova position 2 kyr ago, whereas the broken shell (the yellow dotted ellipse) has been created by the anisotropic giant flare on 1998 August 27. See text for details.

"Star 7" was confirmed by Keck 2 LGS-AO/NIRC2 observation as the IR counterpart (Tendulkar et al. 2012).

Tendulkar et al. (2012) confirmed claimed in Vrba et al. (1996, 2000) physical connection of the magnetar with an young close ($\approx 14''$ ($7''$) to the centre (edge) of the cluster) compact ($R_{cl} \approx 0.4 - 0.6 \text{ pc}$) embedded cluster of massive stars C1 1900+14 (aka SGR 1900+14 Star Cluster (Morales et al. 2013)) with two luminosity-dominated M5 red supergiant stars and an improved in Davies et al. (2009) distance of $d_{cl} = 12.5 \pm 1.7 \text{ kpc}$ and an extinction of $A_V = 12^m.9 \pm 0^m.5$. With the transverse velocity $v_t = 130 \pm 30 \text{ km s}^{-1}$ for this distance it is possible to estimate the age of the magnetar which needs $6 \pm 1.8(3 \pm 0.9) \text{ kyr}$ to exit from its birthplace at the centre (edge) of the cluster.

An additional confirmation of the magnetar-cluster physical connection presents discovered by Wachter et al. (2008) in Spitzer $16 \mu\text{m}$ and $24 \mu\text{m}$ images an infrared elliptical (semi-axes $36'' \times 19''$ or $2.2 \text{ pc} \times 1.2 \text{ pc}$ for the distance of 12.5 kpc) ring or shell around SGR 1900+14 and explained as a dust-free cavity produced in the stellar cluster-connected dusty gas by the giant flare of SGR 1900+14 on 1998 August 27 (Fig. 2). Observed ring dust temperature of $80 - 120 \text{ K}$ and luminosity of $1.2 \pm 0.2 \text{ Jy}$ and $0.4 \pm 0.1 \text{ Jy}$ at $24 \mu\text{m}$ and $16 \mu\text{m}$, respectively, together with the absence of ring signatures at optical, near-IR, radio- or X-ray wavelengths, was explained in a model of a dust heating by the embedded star cluster without the possible presence of a shock wave from the Supernova explosion. Carried out in Natale et al. (2017) 3D dust radiative transfer modelling reproduces observational data in a model of a cavity in a circum-cluster medium with a sharp inner boundary and a molecular cloud-like extinction, with two illuminating red supergiant stars inside the cavity. The necessary total mass of the radiating dust is $M_{dust,out} \sim 2M_{\odot}$ and the gas number density $n_H \sim 10^3 \text{ cm}^{-3}$ (for a dust-to gas ratio of 0.00619).

Resulting high gas number density at the cavity boundary leads to the total mass of gas inside cavity volume ($\sim 13 \text{ pc}^3$) $M_{gas,in} > 400M_{\odot}$ and the outside mass $M_{gas,out} \sim 320M_{\odot}$, or the total mass of a putative molecular cloud $M_{cl} \gtrsim 10^3 M_{\odot}$, but such a molecular cloud is still not observed. In Vizier J/A+A/560/A76 star cluster catalogue (Morales et al. 2013) the cluster C11900+14/SGR 1900+14 is classified as an "OC2: open cluster without gas and without ATLASGAL survey counterpart". In a complete sample of ~ 8000 $M_{cl} \gtrsim 10^3 M_{\odot}$ dense clumps located in the Galactic disk ($5^\circ < l < 60^\circ$) ATLASGAL (Urquhart et al. 2018) an angular separation with the closest clump is of 0.8° (G043.141-00.01), whereas in the all-Galaxy CO survey ($M_{cl} \gtrsim 3 \times 10^3 M_{\odot}$ in the outer Galaxy) (Rice et al. 2016) the closest molecular cloud with $l = 43^\circ.553$, $b = 0^\circ.567$ is of 0.57° away.

2.3. SGR 1900+14 environment in the X-ray band

In the X-ray domain, after the giant flare in 1998 and two re-brightening in 2001 and 2006 SGR 1900+14 returned to minimum flux quiescent level with a typical for magnetars two-component spectrum: a black body component with temperature of $kT = 0.52 \text{ keV}$ and a hard power-law component with photon index $\Gamma = 1.21$. For a column density of $N_H = 1.9 \times 10^{22} \text{ cm}^{-2}$ a bolometric luminosity is of $L_{bol} = 5.6 \times 10^{35} \text{ erg s}^{-1}$ (Turolla et al. 2015; Enoto et al. 2017; Coti Zelati et al. 2018; Tamba et al. 2019). Recent analysis of XMM-Newton and NuSTAR data (Tamba et al. 2019) has revealed a monotonic decrease in the 1 – 10 keV flux and the spin-down rate \dot{P} in 2006-2016. Newly obtained values for 2016 $P = 5.22669(3) \text{ s}$, $\dot{P} = 3.3 \times 10^{-11} \text{ s s}^{-1}$ correspond to improved values of the magnetar magnetic field $B_d = 4.3 \times 10^{14} \text{ G}$ and the characteristic age $\tau_c \approx 2.4 \text{ kyr}$ (cf. with an old value $\tau_c \approx 700 \text{ yr}$). No signatures of an adjacent SNR or MWN were detected yet in the X-ray band.

We adopted the intrinsic (unabsorbed) 2 – 10 keV flux of SGR 1900+14 $F_{2-10 \text{ keV}} = 1.8 \times 10^{-12} \text{ erg cm}^{-2} \text{ s}^{-1} = 1.1 \times 10^{-9} \text{ GeV cm}^{-2} \text{ s}^{-1}$ (Tamba et al. 2019) as an upper limit for expected SNR/MWN 2-10 keV flux.

2.4. SGR 1900+14 environment in the γ -ray band

Recent search for persistent and pulsed γ -ray emission from 20 magnetars (including SGR 1900+14) in six years of *Fermi*-LAT data were also unsuccessful with upper limits $\sim 10^{-12} - 10^{-11} \text{ erg cm}^{-2} \text{ s}^{-1}$ in the 0.1 – 10 GeV band (Li et al. 2017). At the same time, a positive result of this search was revealing of an extended γ -ray source positionally coincident with SGR 1900+14, as well as with the adjacent SNR G042.8+00.6 and SNR G043.5+00.6. In the *Fermi*-LAT Fourth Source Catalogue (Abdollahi et al. 2020) this extended source 4FGL J1908.6+0915e with coordinates $RA = 287^\circ.16$, $Dec = 9^\circ.26$ ($l = 43^\circ.1249$, $b = 0^\circ.4301$), and radius of $\Theta_{HE} = 0^\circ.6$ has an overall significance only 4.58 (Fig. 1). Differential flux density of 4FGL J1908.6+0915e in the 50 MeV – 1 TeV energy range can be approximated by power-law $F(E) = F(E_0)(E/E_0)^{-\Gamma}$ with the reference (pivot) energy $E_0 = 4.52 \text{ GeV}$, the normalization $F(E_0) = (1.01 \pm 0.19) \times 10^{-13} \text{ ph cm}^{-2} \text{ s}^{-1} \text{ MeV}^{-1}$ and the photon index $\Gamma = 2.23 \pm 0.098$. As a likely associated source the SNR G42.8+0.6 is noted.

In the very high energy (VHE, $E > 100 \text{ GeV}$) γ -ray domain the H.E.S.S. Galactic plane survey (H. E. S. S. Collaboration et al. 2018b) reveals a source candidate (hot spot) HOTS J1907+091 with test statistics (TS) above $TS=30$ detection threshold only in one (cross-check $TS=43$) of two analy-

ses (significance of TS=18). Centered at $l = 42^\circ.88 \pm 0^\circ.08$, $b = 0.69^\circ \pm 0^\circ.08$, HOTS J1907+091 has the measured integral flux $F(E > 1 \text{ TeV}) = 4.3 \times 10^{-13} \text{ cm}^{-2} \text{ s}^{-1}$ and extension (radius) of $\Theta_{\text{VHE}} = 0^\circ.17 \pm 0^\circ.04$. For purpose of modelling we approximate the 1 – 10 TeV HOTS J1907+091 differential flux by a power-law spectrum with $\Gamma = 2.3 \pm 0.2$ and $\delta F = 0.2F$ (Figs. 3–7).

HOTS J1907+091 has two potential counterparts: the magnetar SGR 1900+14 and the SNR G42.8+0.6 (H. E. S. S. Collaboration et al. 2018b). Set of objects recently detected in the HGPS significance map around the SGR 1900+14 position using an edge detection operator and a Hough circle transform (Remy et al. 2020) is also presented in Fig. 1.

The closest source to SGR 1900+14 (a separation of $\approx 0^\circ.75$) in the 3HWC HAWC Observatory Gamma-Ray Catalogue (Albert et al. 2020) is a TeV point-like source 3HWC J1907+085 with coordinates RA= $286^\circ.79$, Dec= $8^\circ.57$ ($l = 42^\circ.35$, $b = 0^\circ.44$), (all with $1\sigma_{\text{stat}} = 0^\circ.09$), a somewhat low TS=75.5 peak on an extended background spot (with 2HWC J1907+084* counterpart in the 2HWC catalogue (Abeysekara et al. 2017)).

In the 3HWC peak sensitivity region ($\sim 10 \text{ TeV}$) the best fit parameters of the 3HWC J1907+085 power-law γ -ray spectrum are: the reference (pivot) energy $E_0 = 7 \text{ TeV}$, the normalization $F(E_0) = (8.4^{+0.9+2.5}_{-1.0-1.62}) \times 10^{-15} \text{ TeV}^{-1} \text{ cm}^{-2} \text{ s}^{-1}$ and the photon index $\Gamma = 2.95 \pm 0.09^{+0.04}_{-0.09}$. A shell-like (necklace) structure (with 3HWC J1907+085/2HWC J1907+084* as the brighter knot ($\sigma \sim 5$)), overlapping SGR 1900+14, the SNR G42.8+0.6 and H.E.S.S. HOTS J1907+091, are clearly visible in the γ -ray $\sigma \geq 3$ excess map with subtracted γ -rays from the spatially extended source MGRO J1908+06 (see Extended Data Fig. 1 in Abeysekara et al. (2018)).

To summarise, as the potential observational signatures of SGR 1900+14-connected SNR/MWN we can consider only extended HE and VHE γ -ray sources: the *Fermi*-LAT source 4FGL J1908.6+0915e, the H.E.S.S. source candidate (hot spot) HOTS J1907+091, and similar hot spot around HAWC point-like source 3HWC J1907+085/2HWC J1907+084* (Fig. 1).

3. Supernova and SNR associated with the magnetar SGR 1900+14

3.1. SNR/pulsar wind nebula (PWN) – magnetar associations

Of 29 confirmed or supposed magnetars in the McGill magnetar catalogue (Olausen & Kaspi 2014) only 14 are associated (some likely) with SNRs and a few with PWNe (Ferrand & Safi-Harb (2012), <http://www.physics.umanitoba.ca/snr/SNRcat>; Kaspi & Beloborodov (2017)), in contrast to expectations of a Hypernova scenario owing to a fast loss of $\sim 10^{52}$ erg of rotational energy by new-born $P_i \sim 1 \text{ ms}$ magnetar, both SNRs and PWNe show rather typical of ordinary Supernovae characteristics (see discussion in Kaspi & Beloborodov (2017); Zhou et al. (2019)). So, Zhou et al. (2019) have investigated three magnetar-hosting SNRs: Kes 73, RCW 103 and N49, showing bright, extended X-ray emission and revealed that all of them have low ($< 20M_\odot$) progenitor stars' masses and low to moderate explosion energies (from 10^{50} erg to 1.7×10^{51} erg).

In a similar way, the X-ray luminosities of the PWNe around of five known high-B pulsars and magnetars, alike to an ordinary pulsar case, can be supported by the pulsar spin-down power as well, though a high X-ray efficiency $\eta_{X,PWN} = L_{X,PWN}/\dot{E}_{\text{rot}} \leq 0.4$ (maximum $\eta_{X,PWN} = 0.35$ in the SGR J1935+215 case) is necessary (see Blumer et al. (2017) and references therein).

In the HE – VHE γ -ray domain only two magnetars are recently considered as probably connected with SNRs/PWNe: Swift J1834.9-0846 (the possessor of a X-ray PWN) is coincident with the SNR W41, the GeV source 2FGL J1834.3-0848 and the TeV source HESS J1834-097, while CXOU J171405.7-38103 (a SGR 1900+14 twin, without direct X-ray PWN signatures) is coincident with the SNR CTB 37B, the *Fermi*-LAT point source 4FGL J1714.1-3811 and the TeV source HESS J1713-381 (see Gotthelf et al. (2019) and references therein).

3.2. SNR/PWN models of γ -ray sources in the SGR 1900+14 neighbourhood

As noted above, SGR 1900+14 does not show reliable signatures of SNR and/or PWN counterparts. But such a coincidence of SGR 1900+14 with extended (4FGL J1908.6+0915e, HOTS J1907+091) and point-like (HAWC 2HWC J1907+084*/3HWC J1907+085) HE – VHE γ -ray sources is hardly accidental and may indicate the presence of relativistic hadrons and leptons in SGR 1900+14 outskirts, accelerated in a magnetar-related SNR and/or at a PWN termination shock (TS) during the period of intense spin-down energy losses. So, HOTS J1907+091 with the measured integral photon flux $F_{ph}(E > 1 \text{ TeV}) = 4.3 \times 10^{-13} \text{ cm}^{-2} \text{ s}^{-1}$ ($F_E(E > 1 \text{ TeV}) = 2.3 \text{ TeV} \times F_{ph}(E > 1 \text{ TeV}) = 9.9 \times 10^{-13} \text{ TeV cm}^{-2} \text{ s}^{-1}$ for the spectral index $\Gamma = 2.3$) and an extension of $\Theta = 0^\circ.17 \pm 0^\circ.04$ (H. E. S. S. Collaboration et al. 2018b) can be explained in a hadronic emission scenario with pp interaction of SNR shock-accelerated protons and heavy nuclei with an ISM plasma of number density n_{ISM} . The necessary energy of accelerated cosmic rays (protons) with $E_p > 10 \text{ TeV}$ (in hadronic $E_p \gtrsim 10 \text{ TeV}$ scenario $E_\gamma \approx 0.1E_p$)

$$W_p(E_p > 10 \text{ TeV}) \sim 4\pi d_{\text{mag}}^2 F_E(E > 1 \text{ TeV}) t_{py} \sim 2 \times 10^{50} (n_{ISM}/1 \text{ cm}^{-3})^{-1} \text{ erg}, \quad (1)$$

or the total CR proton energy

$$W_{p,tot} = W_p(E_p > 1 \text{ GeV}) \sim (1 \text{ GeV}/10 \text{ TeV})^{2-\Gamma} \times W_p(E_p > 10 \text{ TeV}) \sim 3 \times 10^{51} (n_{ISM}/1 \text{ cm}^{-3})^{-1} \text{ erg} \quad (2)$$

for $1 \text{ GeV} < E_p < 1 \text{ PeV}$ cosmic ray bubble with typical for Galactic VHE γ -ray sources power-law spectrum (photon index $\Gamma = 2.3$), cooling time for py -channel $t_{py}(E_p = 10 \text{ TeV}) = E_p/\dot{E}_p \sim 5 \times 10^{15} (n_{ISM}/1 \text{ cm}^{-3})^{-1} \text{ s}$ and the radius of $R_{\text{bub}} \approx 35 \text{ pc}$ for the distance to SGR 1900+14 $d_{\text{mag}} = 12.5 \text{ kpc}$.

Similar estimate of $W_{p,tot}$ for HOTS J1907+091 flux follows from the well-known formula for the standard chemical composition of CRs and the ambient gas (Aharonian 2004) $F_{ph}(E > 1 \text{ TeV}) = 0.2 \times 10^{-11} A \text{ cm}^{-2} \text{ s}^{-1}$ for $\Gamma = 2.3$, where A is a scaling parameter

$$A = \frac{W_p}{10^{50} \text{ erg}} \left(\frac{d}{1 \text{ kpc}} \right)^{-2} \frac{n_{ISM}}{1 \text{ cm}^{-3}}. \quad (3)$$

In a leptonic emission scenario with inverse Compton (IC) scattering of background radiation (CMB etc.) by SNR shock-accelerated relativistic electrons or by relativistic e^+e^- pairs accelerated at relativistic TS in PWN with $E_e \gtrsim 10 \text{ TeV}$ (that is, $E_\gamma \approx 4/3\gamma_e^2 E_{\text{CMB}} \approx 0.3(E_e/10 \text{ TeV})^2 \text{ TeV}$, where $\gamma_e = E_e/m_e c^2$ is the Lorentz-factor of electron) and with the CMB photon energy $E_{\text{CMB}} \approx 6 \times 10^{-4} \text{ eV}$ the IC cooling time is $t_{IC}(E_e) =$

$E_e/\dot{E}_e \sim 4 \times 10^{12}(E_e/10 \text{ TeV})^{-1} \text{ s}$ and for an CR lepton spectrum, similar to the proton case, the necessary energy of accelerated leptons is expected to be

$$\begin{aligned} W_e(E_e > 10 \text{ TeV}) &\sim 4\pi d_{\text{mag}}^2 F_E(E > 1 \text{ TeV}) t_{IC} \\ &\sim W_p(E_p > 10 \text{ TeV})(t_{IC}/t_{p\gamma}) \sim 2 \times 10^{47} \text{ erg}, \end{aligned} \quad (4)$$

or the total CR lepton energy

$$\begin{aligned} W_{e,\text{tot}} = W_e(E_e > 1 \text{ GeV}) &\sim 16W_e(E_e > 10 \text{ TeV}) \\ &\sim 3 \times 10^{48} \text{ erg} \end{aligned} \quad (5)$$

(see details of calculations in H. E. S. S. Collaboration et al. (2018)).

An upper limit on measured integral 1 – 10 TeV photon flux $F_{ph}^{ul} = 7.2 \times 10^{-13} \text{ cm}^{-2} \text{ s}^{-1}$ with $\sigma = 4.9$ from a region of $\Theta = 0.3^\circ$ around the SNR G42.8+0.6 (H. E. S. S. Collaboration et al. (2018)), which overlaps HOTS J1907+091, may serve as an additional confirmation of reality of the SGR 1900+14-connected VHE γ -ray source with estimated above characteristics.

In the HE (100 MeV – 100 GeV) band the *Fermi*-LAT extended source 4FGL J1908.6+0915e, overlapping the SGR 1900+14 position, has a power-law spectrum with integral energy flux $F_E(E > 100 \text{ MeV}) = 2.75 \times 10^{-11} \text{ erg cm}^{-2} \text{ s}^{-1}$ and photon index $\Gamma = 2.2$ (Abdollahi et al. 2020). In the hadronic emission scenario with $E_\gamma \approx 0.1E_p$ a requirement for the total CR (proton) energy

$$W_{p,\text{tot}} = W_p(E_p > 1 \text{ GeV}) \sim 2 \times 10^{51}(n_{ISM}/1 \text{ cm}^{-3})^{-1} \text{ erg} \quad (6)$$

is similar to the considered above HOTS J1907+091 case owing to an agreement of HE and VHE spectra (Fig. 3).

In the leptonic-CMB emission scenario the 100 MeV – 100 GeV γ -ray band corresponds to 200 GeV $< E_e < 6 \text{ TeV}$ and a requirement for the CR $E_e \gtrsim 200 \text{ GeV}$ electron energy is

$$\begin{aligned} W_e(E_e \gtrsim 200 \text{ GeV}) &\sim 4\pi d_{\text{mag}}^2 F_E(E > 100 \text{ MeV}) \\ &\times t_{IC}(E_e = 200 \text{ GeV}) \sim 1 \times 10^{50} \text{ erg}, \end{aligned} \quad (7)$$

and for the total CR electron energy we have $W_{e,\text{tot}} = W_e(E_e > 1 \text{ GeV}) \sim 3 \times 10^{50} \text{ erg}$.

Obtained characteristics of the observed HE – VHE sources, namely, the total energy of hadronic ($W_{p,\text{tot}} \sim 2 \times 10^{51}(n_{ISM}/1 \text{ cm}^{-3})^{-1} \text{ erg}$) or leptonic ($W_{e,\text{tot}} \sim 3 \times 10^{50} \text{ erg}$) CRs inside the $R_{\text{bub}} \sim 35 \text{ pc}$ bubble significantly exceed the expected typical SNR values $W_{SNR} \sim 10^{51} \text{ erg}$, $W_{p,\text{tot}} \sim 0.1W_{SNR} \sim 10^{50} \text{ erg}$, $W_e \sim 0.01W_{p,\text{tot}} \sim 10^{48} \text{ erg}$, $R_{SNR}(t \sim 10^3 \text{ yr}) \lesssim 10 \text{ pc}$ (Truelove & McKee 1999; Reynolds 2008) and correspond to an Hypernova case with an additional energy supply from a fast rotating new-born magnetar (Dessart & Audit 2018; Orellana et al. 2018)

3.3. Hypernova/Superluminous Supernova as the SGR 1900+14 progenitor

There are observational evidences of a different confidence level that the SGR 1900+14 progenitor was a Hypernova/Superluminous supernova (SLSN). To begin with, SGR 1900+14 agrees in a sky position, a distance, and an age with the 4 BCE "po star" - the visible by naked eye ($\sim 5^m$) transient (~ 1 month) immovable source - from ancient Chinese record dated 4 BC Apr 24 (Wang et al. 2002; Stephenson & Green 2005). Indeed, for the mentioned above distance $d_{\text{mag}} = 12.5 \pm 1.7 \text{ kpc}$

and visual extinction $A_V = 12^m.9 \pm 0^m.5$ (Davies et al. 2009) the absolute magnitude of Hypernova near to the maximum light is $M = m + 5 - 5 \log(d_{\text{mag}}/\text{pc}) - A_V \approx -23^m$. Estimated value of M is slightly more than in the case of the most luminous Supernova yet found ASASSN-15lh (SN 2015L) with $M_{AB} = -23^m.5 \pm 0^m.1$ (Dong et al. 2016) and is similar to $M \gtrsim -23^m$ SLSNe cases (Moriya et al. 2018; Angus et al. 2019).

Even for a more conservative estimate $A_V = N_H/((2.04 \pm 0.05) \times 10^{21} \text{ cm}^{-2})$ for the first Galactic quadrant (Zhu et al. 2017), so that $A_V = 9^m.3$ from X-ray band suggested value $N_H = 1.9 \times 10^{22} \text{ cm}^{-2}$, the absolute magnitude of the SGR 1900+14 progenitor $M \approx -19^m.4$ is noticeably lower than the typical value for core collapse SNe.

An improved SGR 1900+14 age estimate $\tau_c \approx 2.4 \text{ kyr}$ from new P and \dot{P} data (Tamba et al. 2019) agrees with the "po star" age. Moreover, owing to the death of King Herod in 4BC, Spring 4BC is a preferable time of appearance of the Star of Bethlehem.

The second, more reasonable argument, supporting Hypernova nature of the SGR 1900+14 progenitor is an absence of SNR signatures in radio- to X-ray band *together with* the absence of a molecular cloud (clump) as a component (dominated by mass) of the star cluster C11900+14/SGR 1900+14 (Morales et al. 2013), despite the classification of this cluster as *embedded* in Vrba et al. (2000). In our interpretation, the Hypernova outburst of the most massive star - progenitor of SGR 1900+14 in this embedded cluster led to an expelling of a gas component from the cluster, that is, already the first Supernova outburst turned the embedded star cluster into the "open cluster without gas and without ATLASGAL survey counterpart"(Morales et al. 2013). Moreover, molecular clumps are typically destroyed by a newly formed star backreaction even before a SN era (see discussion in Krumholz et al. 2019; Dinnbier & Walch 2020).

The third argument explains the unexpected presence of the mentioned above IR-radiating dust of total mass $M_{\text{dust,out}} \approx 2M_\odot$ for presupernova wind expelling the initial cluster dust together with the cluster gas. In our model the observed IR ring of radius $R_{\text{ring}} \approx 27'' \approx 1.7 \text{ pc}$ consists of a newly formed dust in the Hypernova ejecta and is centered on the position of the magnetar's birthplace about 2 kyr ago (Fig. 2), supporting the 2 kyr magnetar's age.

The discussed above elliptical fit to the IR ring with ratio of axes $\approx 2 : 1$ (Wachter et al. 2008; Natale et al. 2017) takes an inflated in NW direction part of the ring into account. In our model only this dust-free cavity in the inflated part of ring was produced by the *anisotropic* giant flare in August 1998 (or during the possible previous, even more energetic, giant flare). A short flare duration ($\lesssim 1 \text{ s}$) in comparison with the magnetar's rotational period ($P = 5.2 \text{ s}$) results in an anisotropic energy release with a collimation angle $\sim 1 \text{ rad}$ in an agreement with observations.

The fourth argument is the compliance of the magnetar progenitor star with the requirements of the dust-rich Hypernova remnant (HNR) model. The SGR 1900+14 progenitor mass is estimated to be $17 \pm 2 M_\odot$ (Davies et al. 2009), similar to the relatively low-mass progenitors of the SNR Kes 73 (G27.4+0.0) ($< 20M_\odot$) (Borkowski & Reynolds 2017) and the SNR Kes 75 (G29.7-0.3) ($8 - 12M_\odot$) (Temim et al. 2019).

Core-collapse Supernovae are efficient dust producers (about 3 – 10 % of the total mass of the ejecta) (Sarangi et al. 2018; Micelotta et al. 2018). Marassi et al. (2019) shown, that evolution of a rotating ($V_{\text{rot}} = 300 \text{ km s}^{-1}$) star model with an initial mass $M_{\text{ini}} = 15M_\odot$ and solar metallicity ([Fe/H]=0) ends by a pre-Supernova mass of $M_{\text{preSN}} = 6.22(6.22)M_\odot$ and a Ib SN outburst with an explosion energy $E_{SN} = 0.93(1.2) \times 10^{51} \text{ erg}$,

an ejected mass of $M_{eje} = 4.23(5.21)M_{\odot}$ and a dust mass of $M_{dust} = 1.5(2.25)M_{\odot}$. An additional energy supply from a new-born magnetar with a rotational energy $E_{rot} \approx 2 \times 10^{52} P_{i,-3}^{-2}$ erg will provide a Hypernova type of an explosion (Metzger et al. 2018; Piran et al. 2019).

But the most conclusive arguments follow from an interpretation of HE and UHE γ -ray emission from the SGR 1900+14 region. Below we consider the two main scenarios – hadronic and leptonic – of γ -ray emission generation in a magnetar-related HNR model.

4. Magnetar-related HNR as a VHE γ -ray source

4.1. Evolution and signatures of ordinary magnetar-related SNRs

As follows from the above mentioned data, SGR 1900+14 was born 2 kyr ago as a result of $M \approx 17M_{\odot}$ progenitor SN outburst inside the $M \sim 10^3 - 10^4 M_{\odot}$ young star cluster Cl 1900+14/SGR 1900+14. An ordinary SNR with an explosion energy $E_{SN} \sim 10^{51}$ erg in a dense ($n_{cl} = \rho_{cl}/\mu \sim 10^4 \text{ cm}^{-3}$) molecular (the mean molecular weight $\mu = 1.4m_H$) cloud (clump) of radius of $R_{cl} \sim 0.5$ pc is expected to be at an adiabatic (Sedov - Taylor, ST) stage of evolution.

The beginning of the ST stage is determined by characteristic scales of length R_{ch} :

$$R_{ST}^* = c_1(n, s)R_{ch} = c_1(n, s)M_{eje}^{1/3}\rho_{cl}^{-1/3} \quad (8)$$

and time t_{ch} :

$$t_{ST}^* = c_2(n, s)t_{ch} = c_2(n, s)E_{SN}^{-1/2}M_{eje}^{5/6}\rho_{cl}^{-1/3}, \quad (9)$$

where $c_1(n, s)$ and $c_2(n, s)$ are dimensionless functions of density profiles of an ejecta (with a power-law index n) and an ambient medium (with a power-law index s) (Truelove & McKee 1999).

At the ST stage the time-dependent external (forward) shock wave radius R_{ST} and the velocity D_{ST} are given by

$$R_{ST}(t) = (2.026E_{SN}/\rho_{cl})^{1/5}t^{2/5} \\ = 0.791(E_{SN,51}/n_{cl,4})^{1/5}t_{\text{kyr}}^{2/5} \text{ pc}, \quad (10)$$

$$D_{ST}(t) = (2/5)R_{ST}(t)/t = (2/5)(2.026E_{SN}/\rho_{cl})^{1/2}R_{ST}(t)^{-3/2} \\ = 2.15 \times 10^7 (E_{SN,51}/n_{cl,4})^{1/2}R_{ST,\text{pc}}(t)^{-3/2} \text{ cm s}^{-1} \\ = 3.07 \times 10^7 (E_{SN,51}/n_{cl,4})^{1/5}t_{\text{kyr}}^{-3/5} \text{ cm s}^{-1} \quad (11)$$

(Truelove & McKee 1999; Reynolds 2008).

The next, radiative or pressure driven snowplow (PDS) stage, starts at

$$t_{tr} = 0.069E_{SN,51}^{3/14}n_{cl,4}^{-4/7} \text{ kyr}, \quad (12)$$

$$R_{tr} = 0.27E_{SN,51}^{2/7}n_{cl,4}^{-3/7} \text{ pc}, \quad (13)$$

$$D_{tr} = (2/5)R_{tr}/t_{tr} = 1.53 \times 10^8 E_{SN,51}^{1/14}n_{cl,4}^{1/7} \text{ cm s}^{-1}, \quad (14)$$

$$M_{tr} = 28.9E_{SN,51}^{6/7}n_{cl,4}^{-2/7} M_{\odot}, \quad (15)$$

and at the radiative stage for $1 < t^* = t/t_{tr} < 35$ the SNR evolution is described by

$$R_{rad}(t) = R_{tr} \left(\frac{4}{3}t^* - \frac{1}{3} \right)^{3/10}, \quad (16)$$

$$D_{rad}(t) = D_{tr} \left(\frac{4}{3}t^* - \frac{1}{3} \right)^{-7/10} \quad (17)$$

(Cioffi et al. 1988).

If we use a considered in He et al. (2019) molecular clump model XXS-VC with clump parameters $R_{cl} = 0.7$ pc, $\bar{n}_{cl} = 1.8 \times 10^4 \text{ cm}^{-3}$, $M_{gas} = 1.0 \times 10^3 M_{\odot}$, $M_{star} = 98M_{\odot}$ as a proxy for the star cluster C11900+14/SGR 1900+14, the ordinary $E_{SN} = 10^{51}$ erg SNR enters the radiative stage inside the molecular clump at $t_{tr} \approx 50$ yr, $R_{tr} \approx 0.2$ pc. At present ($t_{SNR} \approx 2$ kyr), the SNR is expected to be at the PDS stage well inside the clump with $R_{rad} \sim 0.7$ pc and should be detectable at different wavelengths in contrast to observational data.

4.2. Evolution and signatures of magnetar-related HNR

For a Hypernova progenitor a non-detection of SNR is quite predicted. Limongi & Chieffi (2018) showed that rotating ($V = 300 \text{ km s}^{-1}$) massive ($M = 15M_{\odot}$) star with solar metallicity ($[\text{Fe}/\text{H}]=0$)¹ spends $t_{WR} = 3.68 \times 10^5$ yr of its life and $M_{w,He} = 4.0M_{\odot}$ of gone with the wind He mass at a WR evolution stage. For a typical WR wind with mass-loss rate $\dot{M}_w \sim 10^{-5}M_{\odot} \text{ yr}^{-1}$, wind velocity $V_w \sim 10^8 \text{ cm s}^{-1}$ and mechanical luminosity $L_w = 0.5\dot{M}_w V_w^2$ the expected time-dependent WR wind bubble radius R_{bub} is (Weaver et al. 1977):

$$R_{bub} = \left(\frac{125}{154\pi} \frac{L_w}{\rho_{cl}} \right)^{1/5} t_w^{3/5} \\ = 8.6 \times 10^{-2} \dot{M}_{w,-5}^{1/5} V_{w,8}^{2/5} n_{cl,4}^{-1/5} t_{w,\text{kyr}}^{3/5} \text{ pc}. \quad (18)$$

In our case $R_{bub} \approx R_{cl} \approx 0.7$ pc for $t_w = 33$ kyr, that is, $t_w \ll t_{WR} = 368$ kyr. It means that the WR wind alone can destroy a molecular clump even before the first SN explosion. So, till the moment of the first SN outburst, joint action of stellar winds of three $M \sim 14 - 18M_{\odot}$ stars in the new-born SGR 1900+14 star cluster can blow-up the gas component of the parent $M_{cl} \sim 10^3 M_{\odot}$ clump up to $\sim 20 - 40$ pc, forming an extended ($\sim 10 - 20$ pc) shell-like halo of fragmented debris of wind bubble shells with the mean number density $n_{sh} \sim 10 \text{ cm}^{-3}$ and the total cluster plus ISM ($n_{ISM} \sim 1 \text{ cm}^{-3}$) swept mass $\sim 10^4 M_{\odot}$ (van Marle & Keppens 2012; Geen et al. 2015; He et al. 2019; Dinnbier & Walch 2020).

In the Hypernova case, the ejecta of $M_{eje} \sim 5M_{\odot}$ will be accelerated by a new-born magnetar with a rotation energy $E_{rot} \sim 10^{52}$ erg up to the velocity $V_{eje} \sim (2E_{rot}/M_{eje})^{1/2} \sim 1.5 \times 10^9 \text{ cm s}^{-1}$ (Woosley 2010; Suzuki & Maeda 2019). Accelerated ejecta will expand in a mix of $n_w \sim 10^{-2} \text{ cm}^{-3}$ winds from the exploded WR-star and the still present in the star cluster two RSG and a few BSG (Davies et al. 2009) stars. Additionally, the wind bubble is expected to be loaded by gas fragments of the original stellar cluster, protruded inside the bubble owing to RT instability of a contact discontinuity, separating the wind and the cluster gas. For a constant ejecta density profile (with power-law index $n = 0$) and a constant density of bubble interior (with

¹ As we mentioned above, such a model provides observed dust mass $M_{dust} \gtrsim 2M_{\odot}$ in the SGR 1900+14 IR shell.

power-law index $s = 0$), thus $c_1(0, 0) = 0.727$, $c_2(0, 0) = 0.495$ (Truelove & McKee 1999)), HNR enters the ST stage at the distance $R_{ST}^* \approx 17$ pc at the time moment $t_{ST}^* \approx 1.1$ kyr and reaches in the ST regime $R_{ST} \approx 24$ pc at the present time $t_{SNR} \approx 2$ kyr, while the reverse shock is at the distance $R_{rs} \approx 16$ pc.

But acceleration of an ejecta shell by a magnetar wind is accompanied by development of the Rayleigh-Taylor instability at a wind bubble-ejecta boundary, which can considerably complicate the process of shell acceleration (Blondin & Chevalier 2017). Recent 3D-modelling of an initial interaction of a powerful MWN ($E_{MWN} \approx E_{rot} \sim 10^{52}$ erg) with a typical Supernova ejecta ($E_{eje} \sim 10^{51}$ erg), presented in Suzuki & Maeda (2019), shows that a considerable wind energy dominance results in the Rayleigh-Taylor instability of the MWN surface, mixing of the relativistic MWN plasma with the Supernova ejecta and destroying a regular shell-like structure of the ejecta. Relativistic jet-like plasma flows penetrate a steep gradient of external ejecta layers with an acceleration of a mildly relativistic forward shock and a subsequent break-out into a surrounding WR wind. This escaping through ejecta channels plasma carries out a dominant part of a magnetar wind energy, living a dense clumpy part of an ejecta with a relatively low energy gain.

In the case of considered in Suzuki & Maeda (2019) ejecta of $M_{eje} = 10M_{\odot}$ a clumpy part of ejecta with a mass $M_{cl} \approx 0.5M_{eje}$ reaches a typical velocity of $\sim 0.01c$ and for the SNR age of 2 kyr will be at distance of ~ 6 pc from the outburst place. In our case of the $M_{eje} \approx 5M_{\odot}$ ejecta, a fragmentation of the ejecta is expected earlier and with lower debris velocities in accordance with the observed SGR 1900+14 IR shell radius of ~ 2 pc.

4.3. Modelling the multiband spectral energy distribution (SED) of the SGR 1900+14 neighbourhood in HNR case

In our Hypernova model the HNR with $E_{HNR} \sim 10^{52}$ erg evolves inside the low-density wind bubble ($n_w \sim 10^{-2} \text{ cm}^{-3}$, $B_w \lesssim 3 \mu\text{G}$) and now ($t_{HNR} = 2$ kyr) is at the ST stage with the radius $R_{HNR} = 24$ pc and the shock velocity $V_{HNR} = 0.4R_{HNR}/t_{HNR} \approx 5000 \text{ km s}^{-1}$, and is approaching an extended ($R \sim 30 - 40$ pc) shell-like halo with $n_{sh} \sim 10 \text{ cm}^{-3}$ and the total swept up mass of $\sim 3 \times 10^4 M_{\odot}$. CR components include hadrons with $W_{cr,p} = 10^{51} \eta_{-1}$ erg and leptons with $W_{cr,e} = 10^{-2} K_{ep,-2} W_{cr,p} = 10^{49} \eta_{-1} K_{ep,-2}$ erg, where η is the efficiency of CR acceleration and K_{ep} is the electron-to-proton energy fraction. Maximum energy of accelerated CRs with the charge Ze in the diffusive shock acceleration at the HNR shock with the shock velocity $V_{HNR} = \beta_{HNR} \cdot c$ and the post-shock magnetic field $B_{HNR} = \sqrt{11} B_w$ is equal to (Hillas 2005):

$$E_{max} \approx \beta_{HNR} Z e R_{HNR} B_{HNR} \\ = 9Z \beta_{HNR,-2} R_{HNR,pc} B_{HNR,\mu\text{G}} \text{ TeV}, \quad (19)$$

or $E_{max} \approx 3Z$ PeV in our case.

The expected spectra of shock-accelerated nuclei (mainly, protons, i=p) and electrons (i=e) are of exponential cut-off power-law type

$$N_i(E_i) = N_{0,i}(E/E_{0,i})^{-\gamma_i} \exp(-E/E_{cut,i}), \quad (20)$$

with $N_e(E) = K_{ep} N_p(E)$, where $K_{ep} \lesssim (m_e/m_p)^{1/2} \approx 0.02$ (Pohl 1993).

Owing to a low density of target nuclei inside the HNR, we expect the main contribution to the observed VHE γ -ray emission of the SGR 1900+14 region from inelastic collisions between shock accelerated and shell-like halo hadrons with

a subsequent neutral pion decay. Shock accelerated electrons will also contribute to the observed VHE γ -ray emission via IC scattering off background photons. Besides the CMB component with temperature $T_{CMB} = 2.7$ K and energy density $w_{CMB} = 0.26 \text{ eV cm}^{-3}$ we consider an infrared ($T_{IR} = 107$ K, $w_{IR} = 1.19 \text{ eV cm}^{-3}$) and a starlight ($T_{SL} = 7906$ K, $w_{SL} = 1.92 \text{ eV cm}^{-3}$) ones as the representative values for the population of TeV PWNe in the H.E.S.S. GPS (H. E. S. S. Collaboration et al. 2018a). Both the hadronic energy loss time for inelastic pp-collisions $t_{pp} \approx 1.7 \times 10^5 (n_{ISM}/1 \text{ cm}^{-3})^{-1}$ kyr and the leptonic cooling time for synchrotron ($w_{MAG} = B^2/8\pi = (B/B_{CMB})^2 w_{CMB}$, where $B_{CMB} = 3.23 \mu\text{G}$) and IC channels $t_i \approx 1.3 \times 10^2 (w_{CMB}/w_i)(E_e/10 \text{ TeV})^{-1}$ kyr ($i = MAG, CMB, IR, SL$) exceed the HNR age for $E_e < 100$ TeV.

Using discussed above *Fermi*-LAT and H.E.S.S. observational data², we have carried out NAIMA-fitting (Zabalza 2015) of SED of the SGR 1900+14 neighbourhood in the HNR model (Figs. 3, 4) and estimated necessary CR parameters and ambient nucleon density (Table 1). As expected from analytical estimates, the main contribution in the observed γ -ray flux provides hadronic mechanism with a high – of Hypernova type – value of CR energy $W_{cr,p} \approx 5 \times 10^{50} (n_{sh}/10 \text{ cm}^{-3})^{-1}$ erg even for swept-up shell with enhanced density ($n_{sh} \sim 10 \text{ cm}^{-3}$). This result is weakly sensitive to the electron contribution (K_{ep}), because the main energy losses occur in the 1 – 10 GeV range.

In the diffusion-reacceleration-convection model (Yuan et al. 2017) the best-fit diffusion coefficient has a form

$$D = D_0(\mathcal{R}/4 \text{ GV})^{\delta}, \quad (21)$$

with $D_0 = 6.14 \times 10^{28} \text{ cm}^2 \text{ s}^{-1}$, $\delta = 0.48$, and with the slope of the injection spectrum of nuclei $\gamma = 2.37$ for $\mathcal{R} > 16$ GV ($\mathcal{R}_{10} = \mathcal{R}/10^{10} \text{ V} > 1.6$). The expected region of HE and VHE γ -ray emission is determined by CR diffusive range (Aharonian 2004):

$$L_{dif} \approx 2(D \cdot t)^{1/2} \approx 35(\mathcal{R}_{10})^{0.24} t_{\text{kyr}}^{1/2} \text{ pc} \quad (22)$$

and corresponds to the observable angular size $\Theta = L_{dif}/d_{mag} \approx 0.5$ for $\mathcal{R} = 3 \times 10^{11} \text{ V}$ and $t_{\text{kyr}} = 2$.

5. Magnetar-related MWN as a VHE γ -ray source

5.1. Gamma-ray PWNe

Ordinary non strongly magnetized ($B_{12} \sim 1 - 10$) new-born pulsars with $P_{i,-2} \sim 1 - 10$ have moderate initial rotational kinetic energies $E_{rot} \sim 2 \times 10^{48} P_{i,-1}^{-2}$ erg, magnetic dipole spin-down luminosities $L_{sd,i} \sim 10^{35} B_{12}^2 P_{i,-1}^{-4}$ erg s^{-1} and spin-down timescale $t_{sd,i} \sim 6 \times 10^2 B_{12}^{-2} P_{i,-1}^2$ kyr. Meantime, typical timescale of young SNR evolution is ~ 10 kyr, therefore a typical pulsar wind of a new-born pulsar interacts generally with a freely expanding Supernova ejecta and forms a PWN between a TS in the free wind and an inner boundary of the shocked ejecta (contact discontinuity) (Gaensler & Slane 2006; Bucciantini et al. 2011; Amato 2014; Blondin & Chevalier 2017; H. E. S. S. Collaboration et al. 2018a; Kargaltsev et al. 2015; Reynolds et al. 2017; Zhu et al. 2018; Amato 2020).

PWNe, especially their TSs, are believed to be effective particle accelerators via diffusive shock acceleration at the TS, as

² The point-like HAWC source 3HWC J1907+085 is not superimposed on the extended *Fermi*-LAT source, its flux is similar to the H.E.S.S. source case.

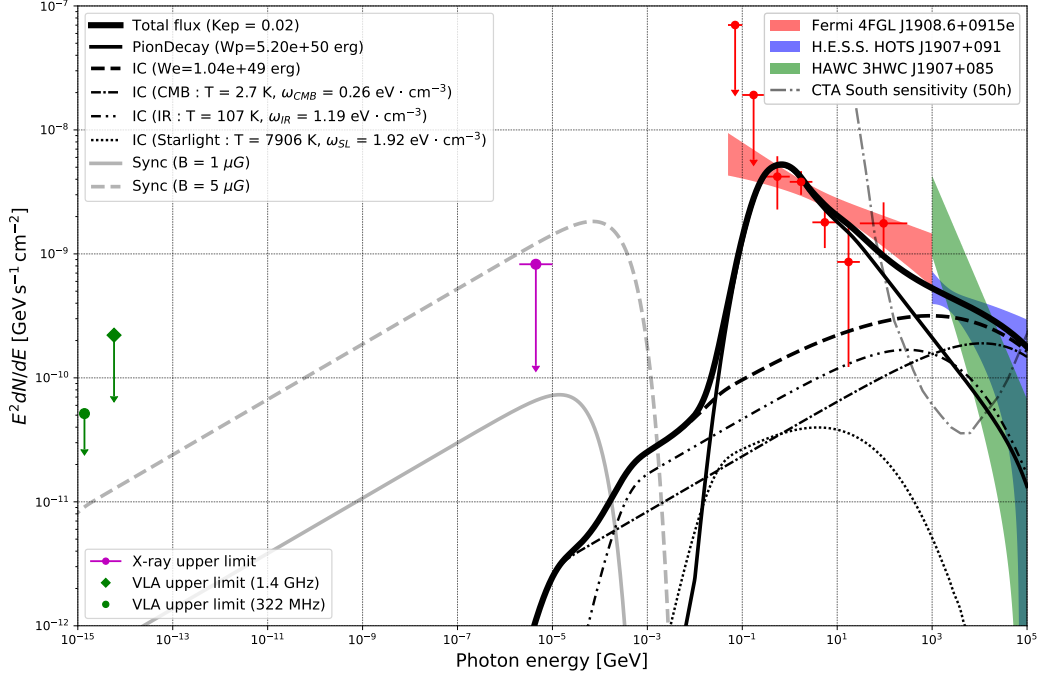


Fig. 3. Modelled SED of magnetar SGR 1900+14 neighbourhood in HNR model. NAIMA-fitted parameters are given in Table 1 (the case of HNR shock accelerated proton and electron power-law spectra with fixed $K_{ep} = 0.02$). Observations of *Fermi*-LAT 4FGL J1908.6+0915e (in red), H.E.S.S. HOTS J1907+091 (in blue) and HAWC 3HWC J1907+085 (in green) are presented together with upper limits in the X-ray (in magenta) and the radio (in green) bands. The total gamma-ray flux is a sum of hadronic (pp-collisions with subsequent neutral pion decay) and leptonic (IC scattering of electrons on CMB, IR and SL background photons) contributions. Synchrotron emission is calculated for two values of the ambient magnetic field – $1 \mu\text{G}$ and $5 \mu\text{G}$. The grey dash-dotted line represents the sensitivity of the CTA South array for a zenith angle $z = 40^\circ$

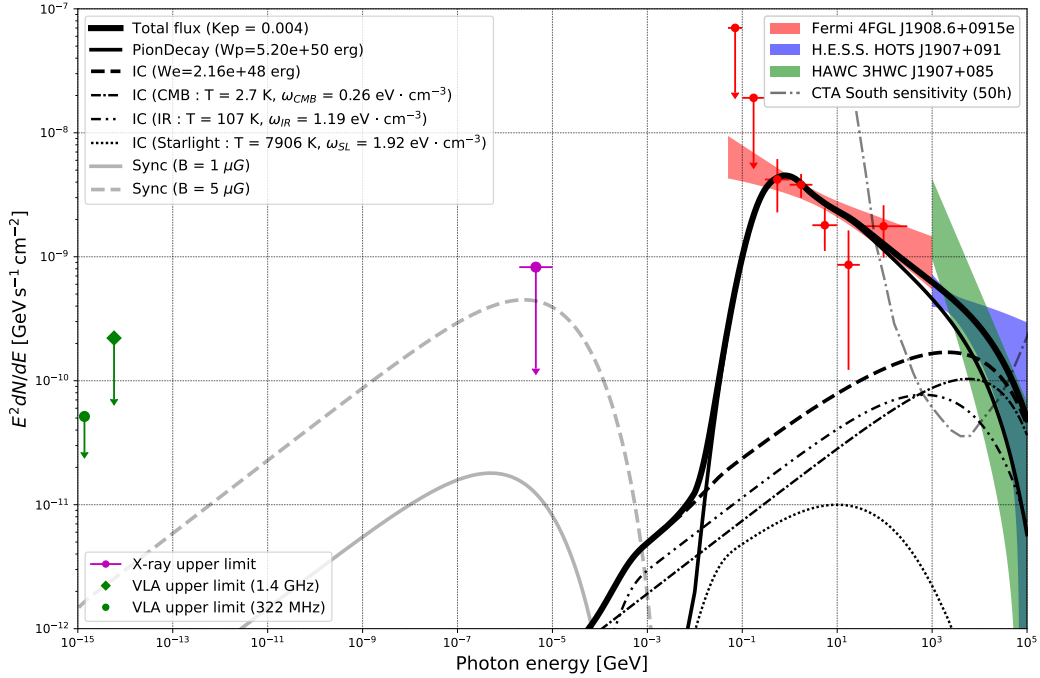


Fig. 4. Same as in Fig. 3 but for exponential cut-off power-law spectra with free K_{ep} .

well as via a driven magnetic reconnection and a resonant absorption of ion-cyclotron waves (Amato 2014, 2020). Accelerated relativistic electrons and positrons (hereafter we use the term electrons to the both electrons and positrons in the PWN case) interact with magnetic and background radiation (CMB,

IR, SL) fields producing synchrotron (in radio- – X-ray band) and IC – SSC (in GeV – TeV band) emission (Gaensler & Slane 2006; Kargaltsev et al. 2015; Zhu et al. 2018; Amato 2020).

If a SNR evolves in the low density ISM, maintaining a high shell velocity for a long time, a PWN expands almost freely in-

side a cold ejecta ($R_{PWN} \propto t^{6/5}$) and can reach a large size. In a case of an anisotropic (asymmetric) SNR owing to an anisotropy of the ISM and/or a SN outburst an anisotropic reverse shock in an ejecta of a middle-age SNR can shift the PWN relative to the pulsar position (de Jager & Djannati-Ataï 2009; Bucciantini et al. 2011; H. E. S. S. Collaboration et al. 2018a). So, of the 14 TeV PWNe in the H.E.S.S Galactic Plane Survey seven have radii larger than 10 pc with similar pulsar offsets (H. E. S. S. Collaboration et al. 2018a). The largest known γ -ray PWN HESS J1825–13 has the intrinsic diameter of $D_{pwn} \approx 100$ pc and the parent young ($\tau_c = 2 \times 10^4$ yr) pulsar PSR B1823-13 (aka PSR J1826-1334) is shifted from the PWN centre by ≈ 33 pc owing to an asymmetric environment (Van Etten & Romani 2011; Khangulyan et al. 2018; H. E. S. S. Collaboration et al. 2019; Principe et al. 2019, 2020).

5.2. Gamma-ray emission of SGR 1900+14 neighbourhood in the magnetar-related MWN model

The PWN HESS J1825–137 is a SGR 1900+14-twin in the VHE γ -ray band with similar sizes, TeV-luminosities, and energy-dependent morphologies, taking a distance ratio 3.93 kpc/12.5 kpc (H. E. S. S. Collaboration et al. 2019; Principe et al. 2019, 2020) into account. But that is allowed to the energetic pulsar PSR B1823-13 with a high spindown luminosity $L_{sd} = 2.8 \times 10^{36}$ erg s $^{-1}$ and a moderate advective PWN velocity $v_{adv} \sim D_{pwn}/2\tau_c \sim 2500$ km s $^{-1}$ is not permitted to the magnetar SGR 1900+14 with a low contemporary spindown luminosity $L_{sd} = 2.6 \times 10^{34}$ erg s $^{-1}$ and a required high advective velocity $v_{adv} \sim D_{mwn}/2\tau_c \sim 60000$ km s $^{-1}$ in a putative relic MWN. It means that the MWN of the required parameters was formed long ago owing to an extremely high spindown luminosity of a new-born millisecond magnetar $L_{sd,i} \sim 2 \times 10^{48}$ erg s $^{-1}$, and an extremely short spindown time scale $t_{sd,i} \sim 10^4$ s for the estimated in Tamba et al. (2019) dipole magnetic field $B_d = 4.3 \times 10^{14}$ G. At the present time $t = t_{mag} = 2$ kyr a magnetar with $L_{sd} = L_{sd,i}(t_{mag}/t_{sd,i})^{-2} = 2.6 \times 10^{34}$ erg s $^{-1}$ cannot effectively support such a MWN.

In contrast to the situation with an ordinary PWN formation via a magnetised electron-positron relativistic wind generation, in our case, for both components of the relativistic outflow from the magnetar - the disk wind and the collimated jet - inside a dense environment of a presupernova envelope, an expected baryon contamination η_{bar} can be considerable. Once more, only some parts, if any, of the relativistic outflow with reduced total energy $E_{esc} = \eta_{esc}E_{rot} \sim 10^{51}\eta_{esc,-1}E_{rot,52}$ erg will successfully penetrate the core part of the stellar envelope and spread in the low density circumstellar environment as a bubble of relativistic plasma, filled by the both leptonic and hadronic components (Piran et al. 2019; Suzuki & Maeda 2019, and references therein).

In the considered above magnetar-connected HNR, accelerated by a disk wind, a penetrated wind energy with $\eta_{esc} \sim 1$ is mainly converted into a kinetic energy of an external part of an ejecta with a mass of approximately several solar masses. Therefore, with additional energy losses due to an adiabatic expansion, parametrized by $\eta_{ad} \sim R_{mwn}/R_{ts}$, a residual energy of relativistic electrons in a diluted MWN inside a Hypernova shell should be presently $E_{mwn} \sim \eta_{lep}\eta_{ad}\eta_{esc}E_{rot} \sim 10^{48}\eta_{lep,-2}\eta_{ad,-2}E_{rot,52}$ erg, where the lepton conversion efficiency $\eta_{lep} = 1 - \eta_{bar}$, that is, only $\sim 10\%$ of the total energy of relativistic electrons accelerated at the HNR shock in considered above case of the magnetar-connected HNR.

More favourable conditions for a powerful MWN formation arise in the case of a relativistic outflow from a magnetar in the form of a collimated jet as it is expected in magnetar-related Hypernovae with possible long GRBs (Piran et al. 2019). In both cases of the break-out a considerable part of magnetar rotational energy will be realised in the form of a bubble of relativistic plasma with baryonic and leptonic components outside an expanding ejecta shell. This bubble, as an analogue of the contaminated by baryons MWN, will expand in a low density ($n_w \leq 10^{-3}$ cm $^{-3}$) cluster stars' wind bubble, supported by a high velocity ejecta as a piston. In this case, at present, the residual energy of relativistic electrons in the MWN *outside* the main Hypernova shell should be

$$E_{mwn} \sim \eta_{lep}\eta_{ad}\eta_{esc}E_{rot} \sim 10^{50}\eta_{lep,-1}\eta_{ad,-1}E_{rot,52} \text{ erg}$$

for $\eta_{ad} \sim R_{HNR}/R_{MWN} \sim 0.1$, $\eta_{esc} \sim 1$, that is, on the order of the total energy of relativistic nuclei accelerated at the HNR shock.

5.3. Modelling the multiband SED of the SGR 1900+14 neighbourhood in the MWN case

We expect that the present relativistic leptonic component of CR in the SGR 1900+14-related MWN is the result of the time-dependent TS acceleration and cooling/escaping/advection processes, analogously to the case of the ordinary PWN (H. E. S. S. Collaboration et al. 2018a; Zhu et al. 2018, and references therein). The observed SED in PWNe is the sum of lepton contributions from different injection epochs and space localisations. In this case a typical exponential cut-off broken power-law injection spectrum

$$N_e(E) = \begin{cases} N_{0,e}(E/E_{0,e})^{-\gamma_{1,e}}, E < E_{br,e} \\ N_{0,e}(E_{br,e}/E_{0,e})^{(\gamma_{2,e}-\gamma_{1,e})}(E/E_{0,e})^{-\gamma_{2,e}} \\ \quad \times \exp(-E/E_{cut,e}), E \geq E_{br,e} \end{cases} \quad (23)$$

with $\gamma_{1,e} < 2$ for $E \leq E_{br,e}$ and $\gamma_{2,e} > 2$ for $E \geq E_{br,e}$, modified to some extent owing to energy losses (mainly at TeV energies), provides an observed bump-like γ -ray emission spectrum with $\nu F_\nu = E^2 F(E)$ maximum at $E \sim E_{bkg}(E_b/m_e c^2)^2 \sim 0.1$ TeV, where E_{bkg} is the energy of background photons (e.g. Ishizaki et al. 2017). For a decreasing $E^2 F(E)$ flux in sub-TeV – TeV region (a photon index $\Gamma > 2$) an effective (average) spectral index of electrons should be $\gamma_{2,e} = 2\Gamma - 1 > 3$. In our case we observe only this post-maximum decreasing $E^2 F(E)$ flux in the all γ -ray GeV – TeV region with $\Gamma \sim 2.2$ (in the GeV-band) – 2.9 (in the TeV-band), therefore we use for modelling the MWN broad band spectrum both an ECBPL model and a inspired by "alternative model" of Ishizaki et al. (2017) PL EC electron spectrum with $E_{min} \sim 10$ GeV and $\gamma_{2,e} > 3$.

The results of the NAIMA-fitting of SED of the SGR 1900+14 neighbourhood in the MWN model for ECBPL and alternative ECPL lepton spectra are presented in Fig. 5 and in Fig. 6, correspondingly. The estimated necessary leptonic CR parameters are presented in Table 1.

Taking a 10-GeV dip in observed *Fermi*-LAT data into account, we consider also the case of two ($i=1, 2$) electron populations with power-law exponential cut-off spectra

$$N_i(E) = N_{0,i}(E/E_{0,i})^{-\gamma_{i,e}} \exp(-E/E_{cut,i}), \quad (24)$$

with $\gamma_{1,e} < 2$ and $\gamma_{2,e} > 2$. SED for this case are presented in Fig. 7 and leptonic CR parameters – in Table 1.

In both cases the observational data can be explained only when the total energy of radiating electrons is $W_{e,tot} \approx 5 \times 10^{50}$ ergs, that is, corresponds to the millisecond period of a new-born magnetar (Table 1).

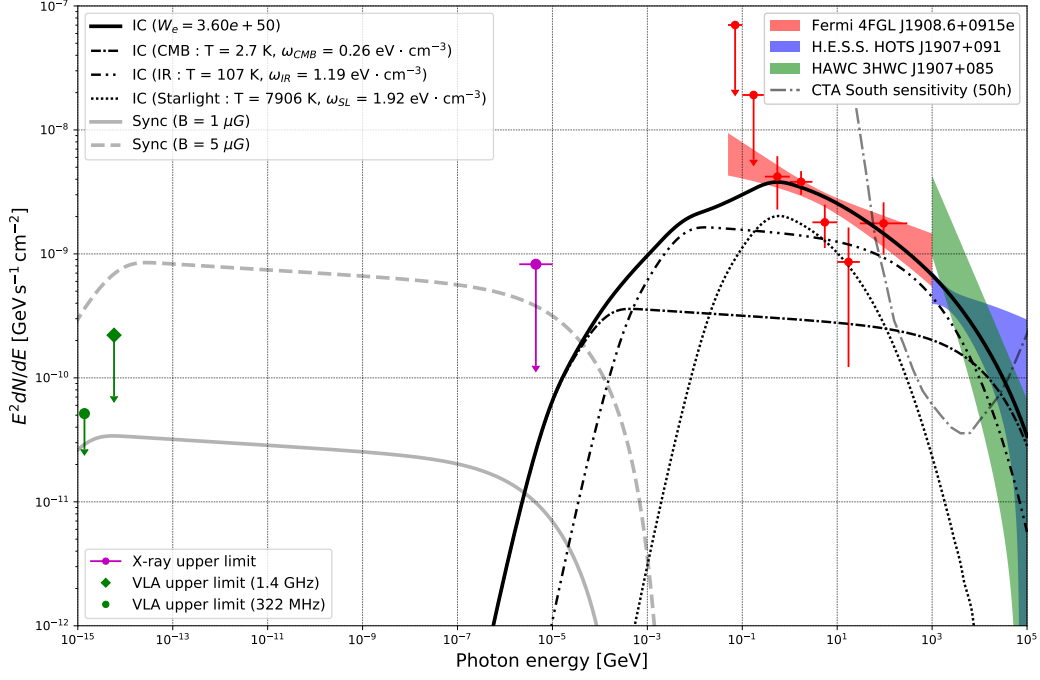


Fig. 5. Modelled SED of magnetar SGR 1900+14 neighbourhood in MWN model. NAIMA-fitted parameters are given in Table 1 (the case of MWN termination shock/reconnection accelerated leptons with an exponential cut-off broken power-law spectrum). The total gamma-ray flux is a sum of contributions from IC scattering of leptons on CMB, IR and SL background photons. The rest of the data is the same as in Fig. 3.

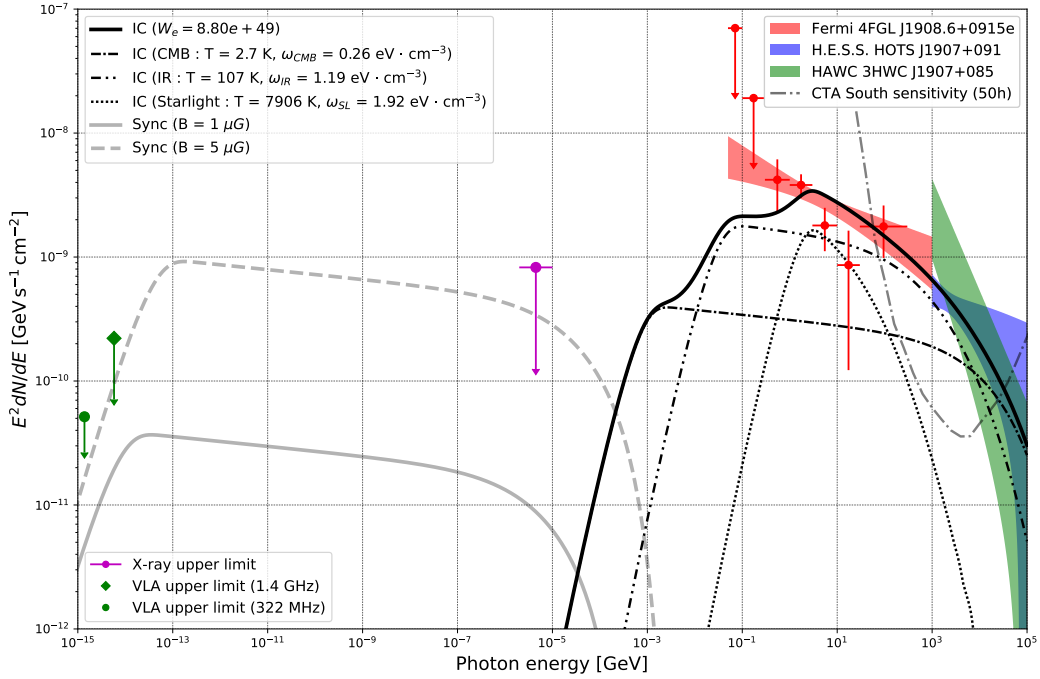


Fig. 6. Same as in Fig. 5 but for alternative exponential cut-off power-law spectrum with $E_{min} = 10$ GeV.

6. Discussion

We have shown that gross characteristics of the observed HE and VHE γ -ray emission from the SGR 1900+14 outskirts together with the absence of detectable emission in lower energy bands can be explained in the framework of the Hypernova-like explosion of a SGR 1900+14 progenitor massive star with a dominant contribution of the new-born fast rotating magnetar in a

Supernova energy reserve. The main requirement for a successful model is a high amount of an energy deposited in accelerated hadrons and leptons in both cases of the γ -ray emission generation: by the dominant contribution of the hadronic mechanism in the HNR model (the necessary total energy of the hadronic CR component is $W_{cr,p} \sim 5 \times 10^{50}$ erg) or by the purely leptonic mechanism in the MWN model ($W_{cr,e} \sim 5 \times 10^{50}$ erg) (Table 1).

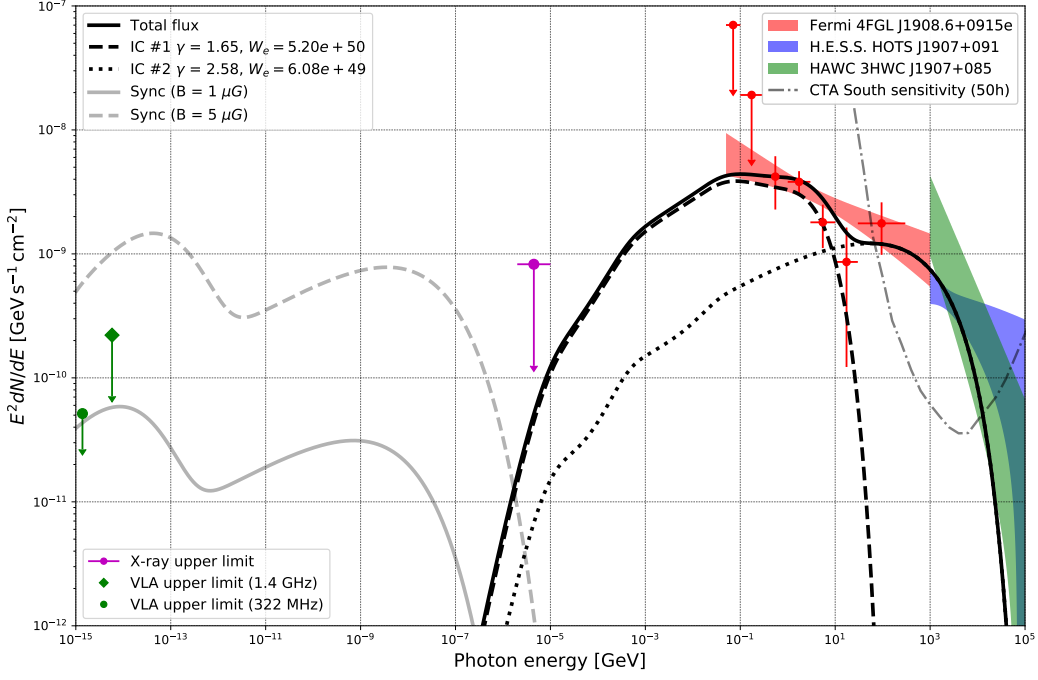


Fig. 7. Same as in Fig. 5 but for two electron populations with exponential cut-off power-law spectra. For both populations only the total gamma-ray fluxes as sums of contributions from IC scattering of leptons on CMB, IR and SL background photons are presented.

Table 1. HNR and MWN NAIMA-fitted models of SED from SGR 1900+14 neighbourhood

Parameter	HNR: PL and ECPL spectra (i=p)		MWN: ECBPL and alternative ECPL spectra (i=e)		MWN: Two electron population spectra (i=e)	
	PL	ECPL	ECBPL	ECPL	ECPL #1	ECPL #2
E_{min} [GeV](fixed)	1	1	1	10	1	1
E_{max} [GeV](fixed)	1e6	1e6	1e6	1e6	1e6	1e6
$N_{0,i}$ [1/eV]	$(1.18 \pm 0.04)e35$	$(1.42 \pm 0.05)e37$	$(1.90 \pm 0.12)e40$	$(8.91 \pm 0.50)e37$	$(4.41 \pm 0.51)e38$	$(8.81 \pm 0.44)e34$
$E_{0,i}$ [TeV]	3.93 ± 0.1	0.78 ± 0.01	0.19 ± 0.01	0.175 ± 0.003	1.91 ± 0.19	1.81 ± 0.19
$E_{br,i}$ [TeV]	-	-	0.0047 ± 0.0003	-	-	-
$E_{cut,i}$ [TeV]	-	185.2 ± 9.5	396.7 ± 41.7	424.3 ± 21.1	0.0096 ± 0.0008	9.99 ± 1.06
$\gamma_{1,i}$	2.55 ± 0.01	2.41 ± 0.03	1.49 ± 0.07	-	1.65 ± 0.11	-
$\gamma_{2,i}$	-	-	3.04 ± 0.06	3.08 ± 0.03	-	2.58 ± 0.17
W_p [erg]	$5.03e50$	$5.12e50$	-	-	-	-
W_e [erg]	$1.04e49$	$2.16e48$	$3.60e50$	$8.80e49$	$5.20e50$	$6.08e49$
n_H [cm $^{-3}$]	11.42 ± 0.66	9.81 ± 0.35	-	-	-	-
K_{ep}	0.02 (fixed)	0.0041 ± 0.0002	-	-	-	-

Whereas the requirement for the high total energy of protons is obvious owing to a relatively low pp-collision frequency ($\sigma_{pp} \ll \sigma_T$), the high total energy of electrons requires explanation. In the VHE γ -ray band both the 1 – 10 TeV luminosity of HOTS J1907+091 ($L_{1-10\text{TeV}} \sim 3 \times 10^{34}$ erg s $^{-1}$ for $\Gamma = 2.3$ (H. E. S. S. Collaboration et al. 2018b)) and the extrapolated spectral luminosity density of 4FGL J1908.6+0915e in the 1 – 10 TeV energy range ($E^2 L_{ph}(E) \sim 1.7 \times 10^{34} (E/1 \text{ TeV})^{-0.23}$ erg s $^{-1}$ (Abdollahi et al. 2020)) correspond to an investigated in H. E. S. S. Collaboration et al. (2018a) *baseline model* describing the evolution of a typical PWN with the initial spin-down luminosity $L_{sd,i} = 2 \times 10^{39}$ erg s $^{-1}$ and the initial spin-down timescale $t_{sd,i} = 0.5$ kyr (the rotational energy reserve $L_{sd,i} t_{sd,i} = 3 \times 10^{49}$ erg corresponds to SGR 1900+14 with initial period $P_i \approx 23$ ms) in a typical spiral-arm environment. The present-day parameters of the baseline PWN – the age $t \approx 5 - 7$ kyr, the radius $R \approx 8$ pc, the magnetic field $B \approx 40 \mu\text{G}$ – are typical for PWNe inside young SNRs (Zhu et al. 2018). In a low-density environment, as in the mentioned above PWN HESS J1825–137 case, PWNe inside the middle-age SNRs can reach a large extension with reduced magnetic fields and re-

spectively low synchrotron luminosities (de Jager & Djannati-Ataï 2009; Van Etten & Romani 2011; Khangulyan et al. 2018; H. E. S. S. Collaboration et al. 2019). In the SGR 1900+14 case some VHE signatures of putative MWN γ -ray emission spectra, namely, the total energy of electrons contributed to the VHE ($E > 0.1$ TeV) γ -ray emission $\lg(E_{tot}/\text{erg}) \sim 48.6$ etc. are typical of bright PWNe with $\lg(E_{tot}/\text{erg}) \sim 47 - 49$ (Giacinti et al. 2020).

But, while the main contribution to the total luminosity L_{PWN} of a typical PWN is provided by the sub-TeV region (a $E^2 F(E) \propto dL_{PWN}(E)/d\ln E$ maximum in sub-TeV region with $E_{PWN,max} \sim 0.1$ TeV), the magnetar-related MWN should have the $E^2 F(E)$ maximum in the GeV region ($E_{MWN,max} \sim 1$ GeV, see Figs. 5, 7).

The main contribution to the IC GeV-photon flux $F_{IC}(E_{IC})$ give relativistic electrons with the Lorentz-factor γ_e , scattering off starlight photons ($E_{SL} \sim 2$ eV, $w_{SL} = 1.92$ eV cm $^{-3}$): $E_{IC} \sim \gamma_e^2 E_{SL}$. The GeV-maximum in the MWN model corresponds to $\gamma_e \sim (E_{IC}/E_{SL})^{1/2} \sim 2 \times 10^4$, that is, $E_{e,GeV} \sim 10$ GeV. Energy losses of one electron $\dot{E} \propto \gamma_e^2$ and of N electrons $\dot{E}N \propto \gamma_e^2 N \propto \gamma_e W_{e,tot}$. Therefore, $E^2 F(E) \propto \gamma_e(E_e(E)) W_{e,tot}$, that is, to maintain similar $E^2 F(E)$ fluxes in GeV ($\gamma_e \sim 2 \times 10^4$) and sub-

TeV ($\gamma_e \sim 2 \times 10^6$) regions the 10 – 100 GeV electron energy should be ~ 100 times higher than the 1 – 10 TeV electron energy and correspond to the new-born millisecond magnetar case $\lg(E_{\text{tot}}/\text{erg}) \approx 50.7$ (Table 1).

7. Conclusions

We have modelled the observed HE and VHE γ -ray emission from the magnetar SGR 1900+14 neighbourhood as a signature of a still undetected magnetar-connected HNR and/or a MWN created by a new-born millisecond magnetar.

Our main conclusions can be summarised as follows.

1. The magnetar-connected Supernova, exploded about 2 kyr ago at distance of 12.5 kpc in the Galactic plane region and mentioned in ancient Chinese records on 4 BC Apr 24, was of a Hypernova type with the explosion energy $E_{\text{HNR}} \approx 10^{52}$ erg.

2. The source of this enhanced explosion energy was the rotational energy $E_{\text{rot}} \approx 2 \times 10^{52} P_{i,-3}^{-2}$ erg of the new-born millisecond strongly magnetised X-ray pulsar – magnetar SGR 1900+14.

3. This energy was contributed to an additional energization of the Hypernova ejecta and to formation of the MWN owing to the extremely high initial magnetic dipole spin-down luminosity. Relative shares of the energy input to the Hypernova ejecta and to the MWN are model-dependent and can be estimated from the analysis of observations.

4. In the HNR model, the energy-dominated Hypernova ejecta with $E_{\text{HNR}} \approx E_{\text{rot}} \approx 10^{52}$ erg evolves inside the low-density wind bubble creating the HNR at the ST stage at present. Shock accelerated nuclei and electrons are diffusively spread over the observed γ -ray regions and γ -ray emission is generated mainly by the hadronic mechanism (pp-collisions with subsequent neutral pion decay) in the dense ($n_{\text{sh}} \sim 10 \text{ cm}^{-3}$) extended shell-like halo of swept up mass of $\sim 3 \times 10^4 M_{\odot}$. In the TeV band the contribution of leptonic mechanism (IC scattering of background CMB, IR and SL photons by shock accelerated electrons) can be dominant.

The main challenge of the HNR model is the requirement of the high value of total cosmic ray energy $W_{\text{cr,p}} \sim 5 \times 10^{50} (n_{\text{sh}}/10 \text{ cm}^{-3})^{-1}$ erg (Table 1, Figs. 3, 4).

5. If the powerful relativistic magnetar wind effectively penetrates the Hypernova ejecta, the resulting energy-dominated MWN with $E_{\text{MWN}} \lesssim E_{\text{rot}} \approx 10^{52}$ erg expands almost freely inside the low-density wind bubble till present. TS/reconnection accelerated electrons and positrons are advectively and diffusively spread over the observed γ -ray regions and γ -ray emission is generated by the leptonic mechanism (IC scattering of background CMB, IR and SL photons by accelerated leptons).

As in the HNR case, the main challenge of the MWN model is the requirement of the high value of the total energy of accelerated leptons $W_{\text{cr,e}} \sim 5 \times 10^{50}$ erg, that is, on the order of the total energy of protons in the HNR model (Table 1, Figs. 5-7).

In both HNR and MWN cases the radio and X-ray non-detection corresponds to a low value of magnetic field $B \lesssim 2 \mu\text{G}$ in the magnetar neighbourhood.

Of course, more realistic model should include contributions from both hadronic and leptonic models, but available sparse observational data do not allow us to build a fully quantitative model for the γ -ray emission of SGR 1900+14 environment. Future observations of the SGR 1900+14 region with the forthcoming Cherenkov Telescope Array (CTA, Cherenkov Telescope Array Consortium et al. (2019) and the Large High Altitude Air Shower Observatory (LHAASO) (Bai et al. 2019) could improve

our understanding of the physical processes in SNRs/MWNe and the nature of the γ -ray emission of SGR 1900+14 neighbourhood.

Acknowledgements. The Spitzer IR image of the SGR 1900+14 environment is shown by courtesy NASA/JPL-Caltech. This work has been supported by scientific program ‘‘Astronomy and space physics’’ of Taras Shevchenko National University of Kyiv (Project No. 19BF023-01).

References

- Aab, A., Abreu, P., Aglietta, M., et al. 2015, *ApJ*, 804, 15
 Abbasi, R. U., Abe, M., Abu-Zayyad, T., et al. 2014, *ApJ*, 790, L21
 Abdollahi, S., Acero, F., Ackermann, M., et al. 2020, *ApJS*, 247, 33
 Abeyssekara, A. U., Albert, A., Alfaro, R., et al. 2018, *Nature*, 562, 82
 Abeyssekara, A. U., Albert, A., Alfaro, R., et al. 2017, *ApJ*, 843, 40
 Aharonian, F. A. 2004, Very high energy cosmic gamma radiation : a crucial window on the extreme Universe
 Albert, A., Alfaro, R., Alvarez, C., et al. 2020, arXiv e-prints, arXiv:2007.08582
 Amato, E. 2014, in International Journal of Modern Physics Conference Series, Vol. 28, International Journal of Modern Physics Conference Series, 1460160
 Amato, E. 2020, arXiv e-prints, arXiv:2001.04442
 Angus, C. R., Smith, M., Sullivan, M., et al. 2019, *MNRAS*, 487, 2215
 Asano, K., Yamazaki, R., & Sugiyama, N. 2006, *PASJ*, 58, L7
 Bai, X., Bi, B. Y., Bi, X. J., et al. 2019, arXiv e-prints, arXiv:1905.02773
 Blondin, J. M. & Chevalier, R. A. 2017, *ApJ*, 845, 139
 Blumer, H., Safi-Harb, S., & McLaughlin, M. A. 2017, *ApJ*, 850, L18
 Borkowski, K. J. & Reynolds, S. P. 2017, *ApJ*, 846, 13
 Bucciantini, N., Arons, J., & Amato, E. 2011, *MNRAS*, 410, 381
 Bucciantini, N., Quataert, E., Arons, J., Metzger, B. D., & Thompson, T. A. 2007, *MNRAS*, 380, 1541
 Cherenkov Telescope Array Consortium, Acharya, B. S., Agudo, I., et al. 2019, Science with the Cherenkov Telescope Array
 Cioffi, D. F., McKee, C. F., & Bertschinger, E. 1988, *ApJ*, 334, 252
 Coti Zelati, F., Rea, N., Pons, J. A., Campana, S., & Esposito, P. 2018, *MNRAS*, 474, 961
 Davies, B., Figer, D. F., Kudritzki, R.-P., et al. 2009, *ApJ*, 707, 844
 de Jager, O. C. & Djannati-Ataï, A. 2009, *Astrophysics and Space Science Library*, Vol. 357, Implications of HESS Observations of Pulsar Wind Nebulae, ed. W. Becker, 451
 Dessart, L. & Audit, E. 2018, *A&A*, 613, A5
 Dinnbier, F. & Walch, S. 2020, *MNRAS*[arXiv:2008.08602]
 Dong, S., Shappee, B. J., Prieto, J. L., et al. 2016, *Science*, 351, 257
 Duncan, R. C. & Thompson, C. 1992, *ApJ*, 392, L9
 Eichler, D. 2005, arXiv e-prints, astro-ph/0504452
 Enoto, T., Shibata, S., Kitaguchi, T., et al. 2017, *ApJS*, 231, 8
 Esposito, P., Rea, N., & Israel, G. L. 2018, arXiv e-prints, arXiv:1803.05716
 Fang, K., Metzger, B. D., Murase, K., Bartos, I., & Kotera, K. 2019, *ApJ*, 878, 34
 Ferrand, G. & Safi-Harb, S. 2012, *Advances in Space Research*, 49, 1313
 Frail, D. A., Kulkarni, S. R., & Bloom, J. S. 1999, *Nature*, 398, 127
 Fuerst, E., Reich, W., Reich, P., Handa, T., & Sofue, Y. 1987, *A&AS*, 69, 403
 Gaensler, B. M. & Slane, P. O. 2006, *ARA&A*, 44, 17
 Geen, S., Rosdahl, J., Blaizot, J., Devriendt, J., & Slyz, A. 2015, *MNRAS*, 448, 3248
 Giacinti, G., Mitchell, A. M. W., López-Coto, R., et al. 2020, *A&A*, 636, A113
 Gnatyk, R. B. 2018, *Kinematics and Physics of Celestial Bodies*, 34, 167
 Gotthelf, E. V., Halpern, J. P., Mori, K., & Beloborodov, A. M. 2019, *ApJ*, 882, 173
 Granot, J., Ramirez-Ruiz, E., Taylor, G. B., et al. 2006, *ApJ*, 638, 391
 Guépin, C. & Kotera, K. 2017, *A&A*, 603, A76
 Guidorzi, C., Montanari, E., Frontera, F., et al. 2001, *GRB Coordinates Network*, 1041, 1
 H. E. S. S. Collaboration, Abdalla, H., Abramowski, A., et al. 2018a, *A&A*, 612, A2
 H. E. S. S. Collaboration, Abdalla, H., Abramowski, A., et al. 2018b, *A&A*, 612, A1
 H. E. S. S. Collaboration, Abdalla, H., Abramowski, A., et al. 2018, *A&A*, 612, A3
 H. E. S. S. Collaboration, Abdalla, H., Aharonian, F., et al. 2019, *A&A*, 621, A116
 He, C.-C., Ricotti, M., & Geen, S. 2019, *MNRAS*, 2162
 Hillas, A. M. 2005, *Journal of Physics G Nuclear Physics*, 31, R95
 Hurley, K., Cline, T., Mazets, E., et al. 1999, *Nature*, 397, 41
 Hurley, K., Montanari, E., Guidorzi, C., Frontera, F., & Feroci, M. 2001, *GRB Coordinates Network*, 1043, 1
 Ishizaki, W., Tanaka, S. J., Asano, K., & Terasawa, T. 2017, *ApJ*, 838, 142

- Kaplan, D. L., Kulkarni, S. R., Frail, D. A., & van Kerkwijk, M. H. 2002, *ApJ*, 566, 378
- Kargaltsev, O., Cerutti, B., Lyubarsky, Y., & Striani, E. 2015, *Space Sci. Rev.*, 191, 391
- Kaspi, V. M. & Beloborodov, A. M. 2017, *ARA&A*, 55, 261
- Kaspi, V. M., Gavriil, F. P., Woods, P. M., et al. 2003, *ApJ*, 588, L93
- Khangulyan, D., Koldoba, A. V., Ustyugova, G. V., Bogovalov, S. V., & Aharonian, F. 2018, *ApJ*, 860, 59
- Kotera, K. & Olinto, A. V. 2011, *ARA&A*, 49, 119
- Kouveliotou, C., Dieters, S., Strohmayer, T., et al. 1998, *Nature*, 393, 235
- Kouveliotou, C., Strohmayer, T., Hurley, K., et al. 1999, *ApJ*, 510, L115
- Krumholz, M. R., McKee, C. F., & Bland-Hawthorn, J. 2019, *ARA&A*, 57, 227
- Li, J., Rea, N., Torres, D. F., & de Oña-Wilhelmi, E. 2017, *ApJ*, 835, 30
- Limongi, M. & Chieffi, A. 2018, *ApJS*, 237, 13
- Liu, X.-W., Wu, X.-F., & Lu, T. 2010, *New A*, 15, 292
- Lorimer, D. R. & Xilouris, K. M. 2000, *ApJ*, 545, 385
- Marassi, S., Schneider, R., Limongi, M., et al. 2019, *MNRAS*, 484, 2587
- Mazets, E. P., Golenetskij, S. V., & Guryan, Y. A. 1979, *Soviet Astronomy Letters*, 5, 343
- Mereghetti, S., Pons, J. A., & Melatos, A. 2015, *Space Sci. Rev.*, 191, 315
- Metzger, B. D., Beniamini, P., & Giannios, D. 2018, *ApJ*, 857, 95
- Micelotta, E. R., Matsuura, M., & Sarangi, A. 2018, *Space Sci. Rev.*, 214, 53
- Morales, E. F. E., Wyrowski, F., Schuller, F., & Menten, K. M. 2013, *A&A*, 560, A76
- Moriya, T. J., Sorokina, E. I., & Chevalier, R. A. 2018, *Space Sci. Rev.*, 214, 59
- Natale, G., Rea, N., Lazzati, D., et al. 2017, *ApJ*, 837, 9
- Olausen, S. A. & Kaspi, V. M. 2014, *ApJS*, 212, 6
- Orellana, M., Bersten, M. C., & Moriya, T. J. 2018, *A&A*, 619, A145
- Paczynski, B. 1992, *Acta Astron.*, 42, 145
- Parfrey, K., Beloborodov, A. M., & Hui, L. 2013, *ApJ*, 774, 92
- Piran, T., Nakar, E., Mazzali, P., & Pian, E. 2019, *ApJ*, 871, L25
- Pohl, M. 1993, *A&A*, 270, 91
- Principe, G., Mitchell, A., Hinton, J., et al. 2019, in *International Cosmic Ray Conference*, Vol. 36, 36th International Cosmic Ray Conference (ICRC2019), 595
- Principe, G., Mitchell, A. M. W., Caroff, S., et al. 2020, *A&A*, 640, A76
- Remy, Q., Gallant, Y. A., & Renaud, M. 2020, *Astroparticle Physics*, 122, 102462
- Reynolds, S. P. 2008, *ARA&A*, 46, 89
- Reynolds, S. P., Pavlov, G. G., Kargaltsev, O., et al. 2017, *Space Sci. Rev.*, 207, 175
- Rice, T. S., Goodman, A. A., Bergin, E. A., Beaumont, C., & Dame, T. M. 2016, *ApJ*, 822, 52
- Sarangi, A., Matsuura, M., & Micelotta, E. R. 2018, *Space Sci. Rev.*, 214, 63
- Sokolosky, P. 2014, Report on workshop “Multimessenger Astronomy in the Era of PeV Neutrinos”, Nov 10-12, 2014, Annapolis, Maryland
- Stephenson, F. R. & Green, D. A. 2005, *Journal for the History of Astronomy*, 36, 217
- Sukhbold, T. & Thompson, T. A. 2017, *MNRAS*, 472, 224
- Suzuki, A. & Maeda, K. 2019, *ApJ*, 880, 150
- Tamba, T., Bamba, A., Odaka, H., & Enoto, T. 2019, *PASJ*, 71, 90
- Temim, T., Slane, P., Sukhbold, T., et al. 2019, *ApJ*, 878, L19
- Tendulkar, S. P., Cameron, P. B., & Kulkarni, S. R. 2012, *ApJ*, 761, 76
- Testa, V., Rea, N., Mignani, R. P., et al. 2008, *A&A*, 482, 607
- Thompson, C. & Duncan, R. C. 1995, *MNRAS*, 275, 255
- Thompson, C. & Duncan, R. C. 1996, *ApJ*, 473, 322
- Truelove, J. K. & McKee, C. F. 1999, *ApJS*, 120, 299
- Turolla, R., Zane, S., & Watts, A. L. 2015, *Reports on Progress in Physics*, 78, 116901
- Urquhart, J. S., König, C., Giannetti, A., et al. 2018, *MNRAS*, 473, 1059
- Van Etten, A. & Romani, R. W. 2011, *ApJ*, 742, 62
- van Marle, A. J. & Keppens, R. 2012, *A&A*, 547, A3
- van Paradijs, J., Taam, R. E., & van den Heuvel, E. P. J. 1995, *A&A*, 299, L41
- Vrba, F. J., Henden, A. A., Luginbuhl, C. B., et al. 2000, *ApJ*, 533, L17
- Vrba, F. J., Luginbuhl, C. B., Hurley, K. C., et al. 1996, *ApJ*, 468, 225
- Wachter, S., Ramirez-Ruiz, E., Dwarkadas, V. V., et al. 2008, *Nature*, 453, 626
- Wang, S., Zhang, C., Jiang, B., et al. 2020, *A&A*, 639, A72
- Wang, Z., Li, Z., & Zhao, Y. 2002, *ApJ*, 569, L43
- Weaver, R., McCray, R., Castor, J., Shapiro, P., & Moore, R. 1977, *ApJ*, 218, 377
- Woosley, S. E. 2010, *ApJ*, 719, L204
- Yuan, Q., Lin, S.-J., Fang, K., & Bi, X.-J. 2017, *Phys. Rev. D*, 95, 083007
- Zabalza, V. 2015, in *International Cosmic Ray Conference*, Vol. 34, 34th International Cosmic Ray Conference (ICRC2015), 922
- Zhou, P., Vink, J., Safi-Harb, S., & Miceli, M. 2019, *A&A*, 629, A51
- Zhu, B.-T., Zhang, L., & Fang, J. 2018, *A&A*, 609, A110
- Zhu, H., Tian, W., Li, A., & Zhang, M. 2017, *MNRAS*, 471, 3494